Atmospheric Environment 303 (2023) 119771

Contents lists available at ScienceDirect

Atmospheric Environment

journal homepage: www.elsevier.com/locate/atmosenv

Nighttime–daytime PM_{10} source apportionment and toxicity in a remoteness inland city of the Iberian Peninsula

Yago Alonso Cipoli [a,b,f,*], Célia Alves [a,**], Marco Rapuano [a,c], Margarita Evtyugina [a], Ismael Casotti Rienda [a], Nora Kováts [d], Ana Vicente [a], Fabio Giardi [e], Leonardo Furst [a,b,f], Teresa Nunes [a], Manuel Feliciano [b,f]

[a] Centre for Environmental and Marine Studies (CESAM), Department of Environment, University of Aveiro, 3810-193, Aveiro, Portugal
[b] Centro de Investigação de Montanha (CIMO), Instituto Politécnico de Bragança, 5300-253, Bragança, Portugal
[c] Department of Chemistry, Alma Mater Studiorum - University of Bologna, Via Zamboni 33, 40126, Bologna, Italy
[d] Centre of Natural Environmental Sciences, University of Pannonia, Egyetem str. 10, 8200, Veszprém, Hungary
[e] INFN - Firenze, National Institute for Nuclear Physics - Florence Division, 50019, Sesto Fiorentino, Italy
[f] Laboratório Associado para a Sustentabilidade e Tecnologia em Regiões de Montanha (SusTEC), Instituto Politécnico de Bragança, 5300-253, Bragança, Portugal

HIGHLIGHTS

- PMF was applied to PM_{10} samples segregated by day and night periods.
- Traffic was found to be the main source during the day representing 33% of the PM_{10}.
- Biomass burning was the main contributor to exceedances of PM_{10} limit values.
- 70% of the samples were classified as toxic.
- Toxicity was mainly attributed to biomass burning.

GRAPHICAL ABSTRACT

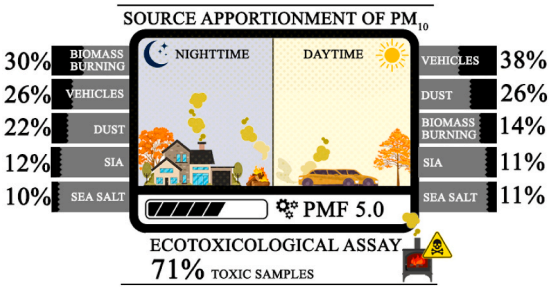

ARTICLE INFO

Keywords:
PM_{10}
PMF
Biomass burning
Bioluminescence inhibition

ABSTRACT

The distribution of daytime and nighttime sources of PM_{10} collected from January to March 2021 at an urban background site in the city of Bragança, Portugal, was performed using positive matrix factorisation (PMF). Additional data of $PM_{2.5}$, NOx and meteorological variables were collected to support the interpretations. A solution with 5 factor profiles was found: traffic (33%), dust (24%), biomass burning (21%), secondary inorganic aerosol (SIA) (12%) and sea salt (10%). Mean daytime and nighttime PM_{10} concentrations were 43.1 μg m^{-3} and 46.1 μg m^{-3}, respectively. Nighttime concentrations were dominated by residential biomass combustion. Vehicle traffic and dust factors showed significantly greater contributions during the day (+12% and +4%, respectively), suggesting that exhaust and non-exhaust emissions and long-range transport are important contributors to daytime PM_{10} levels. In contrast, there were no significant differences between day and night for SIA and sea salt. Exceedances of the daily limit to PM_{10} (50 μg m^{-3}) and $PM_{2.5}$ (15 μg m^{-3}) were observed in 22 (33%) and 27 (40%) days of the campaign, respectively, mostly associated with biomass burning for residential heating, but also with Saharan dust outbreaks. The application of the *Aliivibrio fischeri* bioluminescence inhibition assay for

* Corresponding author. Centre for Environmental and Marine Studies (CESAM), Department of Environment, University of Aveiro, 3810-193, Aveiro, Portugal.
** Corresponding author.
E-mail addresses: yagocipoli@ua.pt (Y.A. Cipoli), celia.alves@ua.pt (C. Alves).

https://doi.org/10.1016/j.atmosenv.2023.119771
Received 6 January 2023; Received in revised form 18 March 2023; Accepted 5 April 2023
Available online 11 April 2023

ecotoxicity assessment allowed classifying 70% of the samples as toxic, especially those from the nocturnal period, indicating that biomass burning is one of the main sources responsible for PM_{10} toxicity. Both the contributions from biomass burning estimated by the PMF and multiple tracers of this source showed statistically significant correlations with the toxicity units.

1. Introduction

Scientific evidence showed an improvement in air quality in Europe over the last decades (Sicard et al., 2021). However, in 2020, the stricter annual air quality guideline of 15 μg m^{-3} set by the World Health Organisation for particulate matter with an equivalent aerodynamic diameter of 10 μm or less (PM_{10}) was exceeded in all reporting European countries, except Iceland (EEA, 2022). Special focus has been given to this air pollutant due to its harmful impacts on climate (Fuzzi et al., 2015; Kanakidou et al., 2005; Ren-Jian et al., 2015) and health (Brook et al., 2010; Chen and Hoek, 2020; Ghosh et al., 2021). A recent Bayesian hierarchical meta-analysis estimated a premature mortality attributed to PM_{10} of 587 per 1,000,000 inhabitants (Waidyatillake et al., 2021). The toxicity of PM, and therefore the effects on health, mainly depend on its physicochemical properties (Crilley et al., 2017). The chemical characterisation of PM has revealed important specificities for each region (e.g., Alves et al., 2018; Pio et al., 2020; Viana et al., 2013; de Miranda et al., 2018; Nava et al., 2020; Zong et al., 2018) highlighting vehicular traffic and biomass burning as the main contributors to PM emissions in urban centres. Characterising in detail the PM chemical composition and source contributions is a crucial prerequisite for the adoption of specific measures leading to the improvement of air quality. Different receptor-oriented models based on statistical analysis of pollutant concentrations measured at a sampling site (receptor site) have been used to identify the source-types and estimate their contributions to the measured levels (Belis et al., 2013). Positive matrix factorisation (PMF) is the most widely used multivariate receptor model (Hopke et al., 2020) since it does not require prior knowledge of sources.

Despite the growing number of studies identifying and quantifying the contributions of common sources (e.g., traffic, fossil fuel combustion and long-range transported dust) of PM in different European regions, such as Barcelona, Spain (Brines et al., 2019), Leece, Italy (Cesari et al., 2018), Patras, Greece (Manousakas et al., 2017), León, Spain (Oduber et al., 2021), London, England (Visser et al., 2015), Po Valley, Italy (Paglione et al., 2020), Paris, France (Srivastavaet al., 2018), and in multiple locations targeted by simultaneous monitoring (Amato et al., 2016; Saraga et al., 2021; Weber et al., 2019), most of them did not differentiate day and night periods. To better understand the pollution patterns, it is advantageous to investigate the day-to-day variability since the strong stability of the atmosphere occurring frequently from late afternoon to late morning in winter contributes to increased PM concentrations compared to the preceding daylight period even if, in general, emissions from sources decrease during nighttime (Vecchi et al., 2007).

Bragança is a small city with weak industrial activities located in north-eastern Portugal near the Spanish border. The influence of traffic emissions and residential biomass combustion on particulate air pollution in the city has been previously reported (Cipoli et al., 2022). However, this study relied on the seasonal and geographical distribution of PM concentrations only during the daytime period, and no source apportionment model was applied. Therefore, with the purpose of deepening the existing knowledge, this work aimed to identify the main sources and their contributions to atmospheric PM during day and night periods, as well as to evaluate the ecotoxicity of PM associated with specific sources. PMF was applied for the first time to daily PM_{10} samples collected during the cold season in an urban background location in Bragança, Portugal. The samples were characterised for their ionic, elemental and carbonaceous composition. PM_{10} ecotoxicity was evaluated by the *Aliivibrio fischeri* bioluminescence inhibition bioassay. The proposed methodology seeks to provide useful information about the main sources that contribute to exceedances of PM_{10} limit values and the toxicity of the samples, which can be used as support for decision making and for implementing plans designed to improve air quality.

2. Material and methods

2.1. Sampling site

The sampling campaign was conducted in 2021 from January 14th to March 17th in Bragança, a small border city with a population of about 35,000 inhabitants located in the extreme northeast of Portugal, in a mountain area at about 700 m of altitude (Pordata, 2021). PM_{10} data were obtained on the roof of the Agricultural High School, on the campus of the Polytechnic Institute of Bragança (41°48′20″ N, 6°45′42″ W, 680 m) at about 15 m above ground level (Fig. 1), in an area located around residential neighbourhoods and main avenues connecting the surrounding rural municipalities to the city centre. The city does not have large emitting industries, and the local contribution to air quality is mainly related to commercial activities, transport and residential heating systems (Cipoli et al., 2022). Another significant source for urban PM levels, as in other regions of the Iberian Peninsula, is the long-range transport of Saharan dust, with frequent intrusions in spring and summer, and few occurrences in the winter periods (Russo et al., 2020).

Bragança has a temperate type of climate Csa (Köppen-Geiger classification, Peel et al., 2007) with dry and hot summers and rainy winters. The average monthly air temperature ranges between 5 °C in December and 23 °C in June, with the highest rainfall and wind speed occurring in January and February, respectively.

2.2. PM_{10} sampling, air quality monitoring and weather data acquisition

Sample collection of PM_{10} was performed by two low-volume samplers (Echo PM TECORA, Italy), operated at a flow rate of 2.3 m^3 h^{-1}, one equipped with quartz fibre filters (2.0 μm pore size, Pallflex®) and the other one with Teflon membrane filters (Pall Corporation), both 47 mm in diameter and pre-weighed. Two samples for each equipment were daily collected in parallel, covering two different periods (08:00 a.m.–06:00 p.m. and 06:30 p.m.–07:30 a.m., local time) in order to determine PM_{10}-bound chemical constituents and their intra-day contributions. The duration of the day and night sampling periods sought to reflect the solar cycle. The daytime period was monitored during sunny hours, when radiation plays an important role in atmospheric photochemistry, while the nighttime period corresponded to the hours without sunlight, coinciding with the accentuation of residential emissions, especially from biomass burning. Blank filters were processed for every ten filters sampled, to ensure the control and quality of the analyses. A total of 102 samples (102 Teflon and 102 quartz) were collected and stored in petri slides, conditioned at −20 °C in a freezer prior to analysis to avoid, as much as possible, any losses of material.

Additionally, a portable weather station (Campbell Scientific Inc., USA) was installed on the roof to collect and record meteorological variables (temperature, relative humidity, precipitation, wind direction and speed). Three gas analysers were used to collect hourly data of CO (model APMA-370, HORIBA, Japan), NO_x (model APNA-370, HORIBA, Japan) and O_3 (model APOA-370, HORIBA, Japan). A β-ray attenuation monitor was used to continuously record $PM_{2.5}$ concentrations (Model F701, VEREWA, Germany).

2.3. Analytical techniques

Gravimetric quantifications of Teflon and quartz filters were performed in a room with controlled relative humidity and temperature (50% and 20 °C) using a 6-digit electronic microbalance (Radwag 5/2Y/F, Poland) with an accuracy of 1 μg. The individual gravimetric concentrations of PM_{10} were obtained from the mean of six weighing with variations less than 40 μg. Two replicate analyses of circular punches of 9 mm of the quartz filters were used to determine the carbonaceous content of PM_{10} samples by a thermal-optical transmission technique, in which organic and elemental carbon (OC and EC) are converted to CO_2 during controlled heating, following the EUSAAR-2 protocol. Heating is performed first in an inert atmosphere of nitrogen, to quantify OC, and then in an oxidising atmosphere (nitrogen and oxygen) to determine EC. The CO_2 released during the heating steps is measured in a non-dispersive infrared analyser. The light transmittance is measured through a laser beam and a photodetector, which allow the separation between the EC formed by pyrolysis of the organic matter during the heating process from the one that was originally present in the sample. The details of this methodology are described elsewhere (Alves et al., 2011; Pio et al., 2011). Teflon filters were split into two parts for different analytical determinations. One half was used to determine elements with Z > 10 (Na, Mg, Al, Si, P, S, Cl, K, Ca, Ti, V, Cr, Mn, Fe, Ni, Cu, Zn, As, Se, Br, Rb, Sr, Y, Zr, Mo, Ba, Pb) by particle-induced X-ray emission (PIXE), as described in detail by Lucarelli et al. (2018). The other portion of the Teflon filter was water-extracted and subjected to analysis of cations (Li^+, Na^+, NH_4^+, K^+, Mg^{2+}, Ca^{2+}) and anions (SO_4^{2-}, Cl^-, PO_4^{3-}, NO_2^-, NO_3^-, F^-, Br^-) by ion chromatography and of anhydrosugars and polyols by high-performance anion-exchange chromatography with pulsed amperometric detection (HPAE-PAD) (Gonçalves et al., 2021).

2.4. Toxicological analysis

The ecotoxic potential of PM_{10} was based on the bioluminescence inhibition of the *Aliivibrio fischeri* (also called *Vibrio fischeri*) bacterium, which when exposed to toxic compounds shows a decrease in its luminous emittance (Kováts and Horváth, 2016). To identify stressor-response patterns, one portion of selected quartz filters (34 samples) was water-extracted, and several dilutions were prepared, following the experimental protocol developed by Kováts et al. (2012). Measurements were conducted using a Luminoskan™ Microplate Luminometer. More methodological details can be consulted in Vicente et al. (2021). The EC_{50} ecotoxicity for each sample (concentration that causes a 50% reduction in bioluminescence production compared to the control test) was calculated using the Ascent software (Aboatox co., Finland). The EC_{50} values were used to calculate the toxicity units (TU), as proposed by Romano et al. (2020). Samples can be classified into four distinct groups based on their TU values: non-toxic (TU < 1), toxic (1 < TU < 10), very toxic (10 < TU < 100) and extremely toxic (TU > 100).

2.5. Enrichment factors

The enrichment factor (EF) was used to identify the contribution of anthropogenic and natural sources to individual elements of PM_{10}. This parameter relates the concentration of an element (Cs) to that of a crustal element (Cref), being a dimensionless parameter given by the following equation:

$$EF = \frac{\frac{Cs}{Cref} \rightarrow PM_{10\ sampled}}{\frac{Cs}{Cref} \rightarrow Crustal} \quad (1)$$

Due to the unavailability of compositional values for the local soil, the calculations were based on the natural abundance (clarkes) in the upper continental crust (Hans Wedepohl, 1995). Aluminum (Al) was used as a normalising reference element, due to its abundance in the earth's crust and its wide application to quantify the enrichment of a potentially contaminant-derived element in an environmental sample relative to the crustal background composition (Alves et al., 2018; Chatoutsidou and Lazaridis, 2022; Khodeir et al., 2012). EFs >10 suggest that anthropic sources contribute to their excess, while EFs <10 indicate a significant proportion of natural (crustal) origin (Biegalski et al., 1998; Nayebare et al., 2018). EFs were calculated for the following elements: Al, Si, Fe, Ca, Mn, Mg, K, Ni, Pb, Cu, Zn, Br.

2.6. Chemical mass closure

The chemical mass closure (CMC) of PM_{10} was performed considering six classes, as follows: secondary inorganic aerosol (SIA), organic matter (OM), elemental carbon (EC), mineral dust (MD), sea salt (SS) and trace elements (TE). The concentration of sea salt was evaluated from the contributions of Na, Cl, Ca, Mg, K and SO_4^{2-} based on the ratio between the ion and Na concentrations, as reported by Calzolai et al. (2014). SIA is composed of NH_4^+, NO_3^- e SO_4^{2-}. Mineral dust

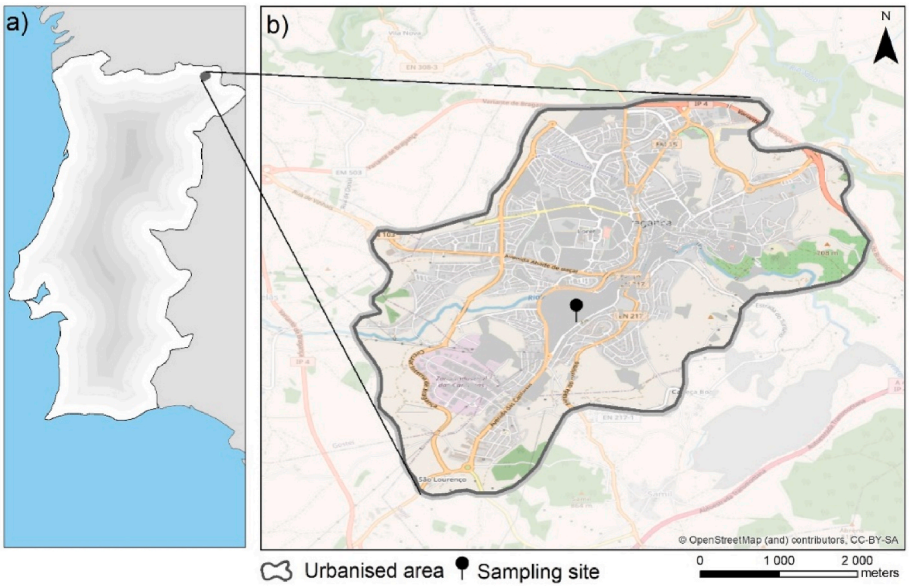

Fig. 1. Location of the sampling site: (a) mainland Portugal, (b) central civil parish in the municipality of Bragança.

concentrations were calculated based on conversion factors for their crustal soil-related metal oxides (Na, K, Mg, Ca, Al, Si, Ti, Fe) (Calzolai et al., 2015). All elements that may originate from sea salt sources were calculated as non-sea salt, based on the difference between the concentrations obtained and those found in sea salt. For this study, a factor of 1.6 was used in the conversion of OC into organic matter (Chow et al., 2015). The concentrations of TE correspond to the sum of all measured elements (in the form of the respective more abundant oxide) that are not classified as marine salt or mineral. The PM_{10} mass closure was then calculated as the sum of all classes. The equations and more details about the calculations can be found in Table S1.

2.7. Positive matrix factorisation

The EPA-provided model known as Positive Matrix Factorisation (PMF version 5.0) was applied to assign the contributions of PM_{10} sources. PMF is a multivariate receptor model, which considers the existence of a relationship between sources and receptor assuming mass conservation (Paatero and Tapper, 1994), as described by the following equation:

$$X_{ij} = \sum_{k=1}^{p} g_{ik} f_{kj} + e_{ij} \quad (2)$$

where X_{ij} is the concentration of jth species measured in the ith sample, p is the total number of factors (independent sources) contributing to the samples, g_{ik} is the relative contribution of the kth factor to the ith sample, f_{kj} is the concentration of jth species from the kth factor profile, and e_{ij} is the residual of the PMF model for the jth species measured in the ith sample. PMF uses the least squares method to estimate the contributions of g_{ik} and f_{kj}, being adjusted until a minimum value of Q for the chosen number of factors. The elements g and f are constrained to be non-negative. The object function Q is defined as:

$$Q = \sum_{j=1}^{m} \sum_{i=1}^{n} \frac{e_{ij}^2}{s_{ij}^2} \quad (3)$$

where s_{ij} is the uncertainty of jth species concentration in the ith sample, m is the number of species and n is the number of samples. Data uncertainties were estimated following the methodology proposed by Polissar et al. (1998). Species with concentrations below the detection limit ($<DL$) were calculated as $\frac{1}{2} * DL$ and relative errors as $\frac{5}{6} * DL$ in accordance with best practices (Norris and Duvall, 2014). Missing values were replaced by the median of available data, while the uncertainty value was four times the median concentration.

PMF includes a weighted scheme considering the uncertainties and concentrations measured point by point, allowing to reduce the weight of any species concentration measurement as a function of signal/noise (S/N) and on prior knowledge of analytical measurements. The variables evaluated as 'weak' had their uncertainties tripled by the model, giving less weight in the final analysis. The species that presented more than half of the concentrations below DL (V, Ti, Se, Rb, Sr, Y, Zr, Mo, Ba) were directly categorised as 'bad', being excluded by the PMF from the rest of the analyses.

Several runs with the PMF were applied in robust mode to analyse the result of base runs (100 runs applied) with varying numbers of sources (from 4 to 10). For each run, the Bootstrap (BS) and Displacement (DISP) methods were used to evaluate the uncertainties associated with the output sources. A 10% extra modelling uncertainty was chosen to find the best solution. Sources were identified and categorised based on PM_{10}-bound chemical constituents in certain factor profiles. More statistical details can be found in the supplementary material (Tables S2–S4).

2.8. Tracing local sources and long-range transport with polar plots and backward trajectories

The relationship between PM_{10} concentrations for each source identified by the PMF as a function of local meteorological parameters and directional dependences from different sources can be demonstrated through bivariate concentration polar plots techniques (Carslaw and Ropkins, 2012). Bivariate polar plots have proven to be extremely valuable for obtaining information and understanding wind speed dependence and direction of sources of atmospheric pollution, being widely used in source apportionment studies (Lucarelli et al., 2020; Miller et al., 2019; Oduber et al., 2021). Pollutants emitted from far locations or higher elevations from the monitoring site require higher wind speeds to facilitate their transport to the sampling site, whereas lower wind speed promotes the accumulation of pollutants primarily originating from the vicinity of the sampling site (Yu et al., 2004).

To better understand the PM_{10} regional transport, backward trajectories were calculated using the Hybrid Single-Particle Lagrangian Integrated Trajectory (HYSPLIT 4.0) model (Rolph et al., 2017) from the National Oceanic and Atmospheric Administration (NOAA), using the isobaric vertical velocity option to identify any Sahara dust intrusion event and maritime influences on PM_{10} samples. The 6 day-back trajectories were calculated using the Global Forecast System Reanalysis (0.25°, global) to obtain meteorological data. The days analysed correspond to periods of elevated concentration (>90th percentile) of soil dust (Al, Si, Ca, Fe) and sea salt (Na, Cl) to verify any connection between the origin of the air masses and their contributions to the PM_{10} levels.

2.9. General statistical analysis

PM_{10} concentration data and its constituents were statistically analysed using SPSS software (IBM Statistics software v. 24). Nonparametric methods were used to evaluate the differences between periods (Mann-Whitney) and the correlation between constituents (Spearman), to obtain statistically significant differences at a confidence level of 95% ($p < 0.05$). The Openair package (version 2.10) and PerformanceAnalytics (version 2.0.4), both available in the R software, were used for plotting pollution roses and correlation graphs, respectively.

3. Results and discussion

3.1. Daily pollutant concentrations and meteorological conditions

The sampling campaign was carried out in the cold period with daily temperatures ranging from −2.8 °C to 13.2 °C and the predominant wind direction during the campaign was from West-Southwest (235°). In approximately 30% of the sampling days, rainfall was recorded (Prec. > 0 mm). The continuous NO_x and $PM_{2.5}$ concentrations and the PM_{10} determined gravimetrically are depicted in Fig. 2. The concentration of pollutants was strongly affected by meteorological conditions, mainly by wind speed and precipitation. PM_{10} data are missing for the period from February 2nd to February 12th. In this period of intense precipitation and strong winds, the sampled filters were discarded because their masses were close to those of the blanks, making further analysis unfeasible. In early February, wind speed reached a maximum of 6.6 m s^{-1}, and the maximum precipitation intensity was about 6.7 mm h^{-1}, favouring wet deposition of PM_{10} and resulting in low concentrations (Table S5).

The maximum hourly concentration (55.65 ± 14.3 μg m^{-3}) and maximum daily average (40.1 ± 5.76 μg m^{-3}) of NO_2 did not exceed the limit values of 200 μg m^{-3} (1-hr standard) and 50 μg m^{-3} (24-hr standard), respectively, imposed by the European Air Quality Directive (2008/50/EU). In particular, the daily cycles for $PM_{2.5}$, NO, NO_2 and NO_x (Fig. S1) exhibited a bimodal structure with peak concentrations coinciding with rush hour traffic periods. However, while the morning

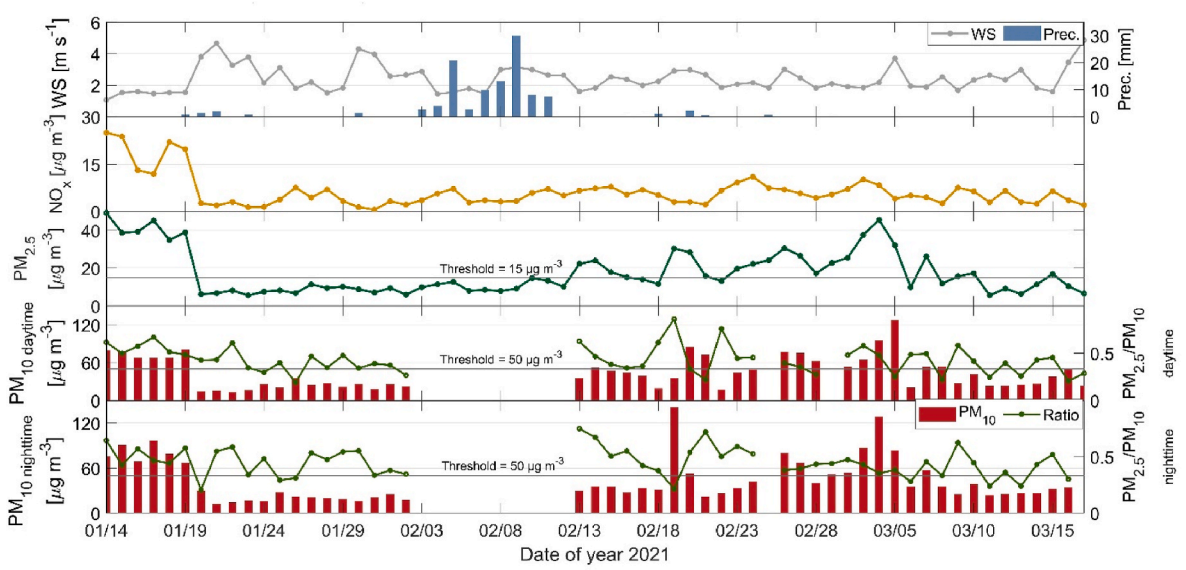

Fig. 2. Daily variation of wind speed (WS), precipitation (Prec), NOx, $PM_{2.5}$ and PM_{10} concentrations for the sampling periods.

peak is almost exclusively related to traffic, schools, commercial establishments and other work activities, the more intense afternoon peak has an additional contribution: domestic emissions from residential heating.

Significant correlations were found between gravimetric concentrations of PM_{10} and $PM_{2.5}$ ($r^2 = 0.92$ with $p < 0.05$) (Fig. S2). On average, the $PM_{2.5}$ concentrations represented 45% of the concentrations obtained by the reference method, with a mean of 17.1 ± 10.8 μg m^{-3} for the whole period. The $PM_{2.5}/PM_{10}$ ratio showed significant differences for the nighttime (0.49) and daytime (0.42) periods, which can be explained in part by the wind regimes (57% weaker at night) and the presence of sources that contribute to the emission of fine particles (e.g., biomass combustion). The daily mean concentrations of $PM_{2.5}$ exceeded the guideline value of 15 μg m^{-3} recommended by the World Health Organisation (should not exceed more than 3–4 days per year) for 27 days during the measurement campaign. PM_{10} concentrations as a function of some meteorological parameters can be seen in Fig. 3. The highest concentrations were registered with lower wind speeds, which favour the accumulation of air pollutants, along with low temperatures and a stable atmosphere. The PM_{10} mean concentration was 44.5 ± 23.6 μg m^{-3}, with higher mean values for nighttime (46.1 ± 25.3 μg m^{-3}) compared to the daytime (43.1 ± 22.0 μg m^{-3}). During the sampling campaign, 22 days showed exceedances of the daily air quality level of 50 μg m^{-3} (Directive, 2008/50/EC).

3.2. Chemical composition and PM_{10} mass closure

The mean concentrations of major PM_{10} constituents are summarised in Table 1. Statistically significant differences were observed between daytime and nighttime for K, levoglucosan, EC, and OC ($p < 0.05$), reinforcing once more that specific sources may be enhanced during different periods. As K and levoglucosan are tracers of biomass burning (Vicente and Alves, 2018), this may be due to domestic emissions generated at nighttime, with higher values for K (1.3 times) and levoglucosan (2.2 times) compared to the daytime. In addition, the OC/EC

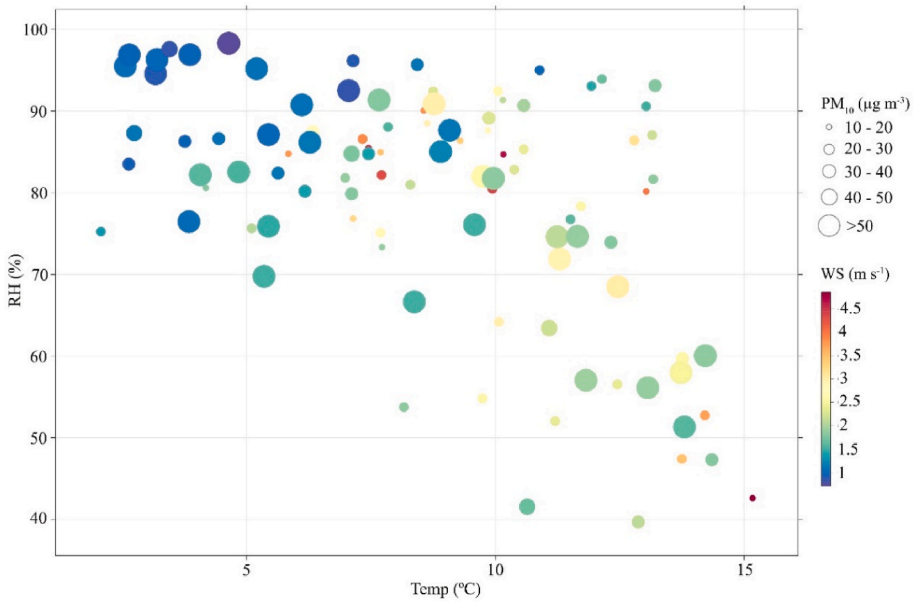

Fig. 3. PM_{10} concentrations as a function of temperature (Temp), relative humidity (RH) and wind speed (WS) for the evaluation period.

Table 1
Summary of PM_{10} concentrations and chemical composition for the entire campaign and segregated by night- and daytime periods and p-values for the comparison between these two periods. PM_{10} CMC refers to the concentration resulting from the sum of OM + EC + SIA + MD + SS + TE. RM is the reconstructed mass in percentage.

Chemical constituents	Whole period (n = 95)			Daytime (n = 49)			Nighttime (n = 46)			p-value
	Mean	Min	Max	Mean	Min	Max	Mean	Min	Max	
μg m^{-3}										
$PM_{10\ gravimetric}$	44.5	12.4	141.2	43.1	13.56	141.2	46.1	12.4	127.7	0.76
SO_4^{2-}	0.78	<DL	2.79	0.71	<DL	2.79	0.87	<DL	2.61	0.28
NO_3^-	1.26	0.08	6.93	1.09	0.08	6.93	1.44	0.09	5.48	0.20
NH_4^+	0.37	<DL	2.28	0.31	<DL	2.28	0.43	<DL	1.73	0.04
OC	7.67	<DL	30.4	6.19	<DL	29.8	9.14	<DL	30.4	0.02
EC	1.86	<DL	8.52	1.61	<DL	8.52	2.11	<DL	8.18	0.03
Levoglucosan	0.79	<DL	4.88	0.45	<DL	3.91	1.16	<DL	4.88	$1.02\ 10^{-4}$
Mannosan	0.05	<DL	0.32	0.03	<DL	0.24	0.08	<DL	0.32	$3.49\ 10^{-4}$
Galactosan	0.04	<DL	0.23	0.02	<DL	0.17	0.05	<DL	0.23	$6.07\ 10^{-5}$
Na	0.56	0.01	3.08	0.58	0.01	2.38	0.54	0.05	3.08	0.95
Mg	0.27	0.01	2.09	0.28	0.01	2.09	0.26	0.02	1.37	0.98
Al	0.89	0.01	8.52	0.91	0.01	8.52	0.86	0.00	7.82	0.69
Si	1.93	0.01	18.3	1.99	0.02	18.3	1.85	0.01	17.7	0.51
Cl	0.53	0.01	3.79	0.49	0.01	2.91	0.57	0.02	3.79	0.76
K	0.47	0.04	2.01	0.39	0.04	2.01	0.56	0.06	1.80	0.03
Ca	0.47	0.01	5.34	0.51	0.00	5.34	0.43	0.01	3.70	0.17
Fe	0.43	0.01	3.84	0.43	0.01	3.84	0.42	0.01	3.33	0.92
ng m^{-3}										
Mn	9.34	<DL	64.2	9.51	<DL	64.2	9.16	<DL	63.3	0.04
Ni	0.81	<DL	3.54	0.82	<DL	2.34	0.77	<DL	3.54	0.85
Cu	2.12	<DL	8.98	2.05	<DL	8.98	2.21	<DL	7.97	0.38
Zn	9.96	1.26	39.8	8.88	1.38	27.5	11.2	1.26	39.8	0.94
Br	2.58	<DL	6.95	2.34	<DL	6.07	2.84	<DL	6.95	0.80
Pb	3.11	<DL	19.2	2.56	<DL	19.2	3.71	<DL	14.3	0.51
Chemical mass closure *(μg m^{-3})*										
OM + EC	22.3	3.83	77.0	26.1	5.03	75.9	15.5	3.83	65.7	0.01
SIA	3.9	0.12	11.2	4.15	0.12	11.2	3.64	0.18	10.9	0.59
MD	11.9	0.26	79.4	11.9	0.50	79.4	11.9	0.26	48.6	0.71
SS	1.03	0.01	5.28	0.96	0.06	3.37	1.16	0.01	5.28	0.89
TE	0.21	0.02	0.49	0.22	0.03	0.49	0.21	0.02	0.43	0.62
$PM_{10\ from\ CMC}$	39.4	7.29	107.7	30.2	7.29	82.9	43.41	9.73	107.7	0.68
RM (%)	87.3	44.3	98.5	89.1	44.1	96.5	85.4	48.3	98.5	

ratio during nighttime of 3.72 is in the range of values reported from residential biomass combustion (Vicente and Alves, 2018). Interestingly, the concentration of Cl during the night was higher than during the day. The mean Cl/Na night ratio of 1.61 was significantly different from that observed in the daytime (0.65). The lower Cl concentrations during the day may be related to its depletion through reactions with nitrate (Contini et al., 2014). Together with K and Cl, SO_4^{2-}, NO_3^-, and NH_4^+ exhibited similar diurnal patterns with a nighttime maximum and a lower daytime concentration. On average, the nocturnal increment in concentrations was 44, 16, 23, 32 and 39%, respectively. Lower mixing layer height at night would be beneficial for the accumulation of pollutants, whilst the elevation of the mixed layer height in the morning could promote the dispersion of pollutants. Also, higher humidity values at night could accelerate the particulate phase formation of these ions (Han et al., 2016). On the other hand, the lower ambient temperatures at night shift the gas-particle equilibrium to the particulate phase (Galindo and Yubero, 2017). As previously observed in Milan (Vecchi et al., 2007), higher concentrations of elements associated with non-exhaust emissions from traffic, such as Zn and Cu, were also recorded at night. The main crustal elements (Al, Si, Fe, Ca, and Mg) reached their highest concentrations in March, when dust transport from North Africa was observed.

The PM_{10} from the mass closure showed a good correlation with the gravimetric PM_{10} concentrations ($r^2 = 0.93$), being able to reconstruct, on average, 87.3% of the total mass. The carbonaceous fraction (OM + EC) was responsible for the greatest mass contribution to PM_{10}, corresponding to 51.8%. All carbonaceous components experienced an increment from day to night (OM +24% and EC +10.5%). According to the results of Ram and Sarin (2011), higher OC and EC concentrations at night are due to: i) an increase in the source strength of carbonaceous species, especially biomass burning, and ii) trapping of aerosols resulting from the decrease in the height of the boundary layer.

Slightly lower concentrations of crustal-related elements were observed at night. This is likely due to the fact that they are mainly in the coarse PM_{10} fraction and are characterised by a higher deposition velocity. Furthermore, during nighttime, the resuspension of particles from the soil is less efficient because of the lower intensity of natural and anthropogenic resuspension processes and the higher humidity of foggy nights usually taking place under wintertime atmospheric stability conditions (Vecchi et al., 2007).

Mineral dust was the second most significant contribution (20.6%) to the PM_{10} mass concentration. Maximum concentrations of crustal elements, such as Si (18.3 μg m^{-3}), Fe (3.84 μg m^{-3}), Ca (5.34 μg m^{-3}) and Al (8.52 μg m^{-3}), observed during the day (February 19th), were associated with Saharan dust intrusion events (Fig. S5). Secondary inorganic aerosols contributed 8.8% to PM_{10}. The sum of cations and anions on an equivalent basis showed a ratio (cations/anions) of 0.92, which indicates an almost neutrality of the aerosol and that the main water-soluble ions that make up the particulate matter were analysed in this study. The slight deficit of cations is possibly related to H^+, which was not analysed directly on the samples. During African outbreaks, an anion deficit (cations/anions = 1.21) was found, as a result of increased Ca^{2+} levels. Significant correlations were found between SIA constituents, suggesting that NH_4^+ acts as a neutraliser of SO_4^{2-} and NO_3^- (Tables S6–S7). Furthermore, the molar ratio between NH_4^+ and SO_4^{2-} (3:1) and NH_4^+ and NO_3^- (1:1) indicates the presence of sufficient NH_4^+ to act as a precursor to form $(NH_4)_2SO_4$ e NH_4NO_3 secondary aerosols (Behera et al., 2013). Less expressive contributions were obtained from

sea salt (5.6%) and trace elements (0.6%) to the PM_{10}. The other unexplained 12.7% mass can be attributed to measurement errors, unanalysed constituents, volatilisation of organic matter and particle-bound water.

3.3. Enrichment factors

The mean enrichment factors for the night and daytime periods are shown in Fig. 4. Of all the trace elements, Br showed the highest EF (449), followed by Zn (93), Cu (72) and Pb (65), indicating a mostly anthropogenic origin. Pb, Cu, Zn, and Cr have been used as tracers of both exhaust and non-exhaust vehicle emissions, especially from tyre and brake wear, and from engine oil impurities (C. A. Alves et al., 2020; Panko et al., 2018). In the past, Br was commonly used as an additive in leaded gasoline (Thomas et al., 1997), which was banned over a decade ago. Since leaded gasoline has been phased out, a decline in Br concentrations would be expected. However, this element can be emitted by several other anthropogenic activities: electric batteries and cars (Gao et al., 2020; Hannan et al., 2017), agricultural pesticides (Shomar, 2006) and water treatment (Winid, 2015). EFs below 10 were found for Al, Si, Fe, Ca, Mn, Mg, and K, suggesting that these elements have a crustal origin. However, outliers (90th percentile = 32) were found for K, more specifically during the nighttime, which indicates that anthropogenic sources, such as biomass burning, may be contributing to the enrichment of this element.

Trace elements related to road traffic (Zn, Cu, Pb) showed statistically significant correlations with each other, as well as crustal elements such as Al, Fe, Si, Ca, and Mg. Bromine and nickel did not present high correlations with other elements, suggesting different emission sources. Interestingly, a strong correlation was observed for Zn with K. In addition to traffic-related emissions, Zn can also become enriched in the fine particle fraction during biomass combustion. Zn is one of the most abundant transition metals in woody fuels, with concentrations between 1 and 300 mg kg^{-1}. During biomass combustion, a large percentage of this element is released into the emission gas as elemental Zn-vapour, which afterwards becomes oxidised to form ZnO ultrafine particles (Uski et al., 2015, and references therin).

3.4. Source apportionment

After careful inspection of the dataset and analysis of the diagnostic results, 95 samples were selected, with 17 species classified as strong and 6 as weak. To determine the number of sources, different configurations were tested. In the case of a 4-factor solution, no complete source profiles were found, while solutions with ≥6 factors presented complex interpretations, indicating mixtures of factors for the same profile. Therefore, a total of 5 sources was chosen presenting interpretable profiles with physical meanings and with values of Q_{robust} and Q_{true} of 1722 and 1739, respectively, in the optimised number of factorial solutions. F-peak equal to zero was used since rotation did not improve data interpretability and Q values. The scaled residues for most species were concentrated within the ±3 SD range with the random distribution of positive and negative values. The chemical profiles and their contributions to the PMF solution are detailed in Fig. 5. They were categorised as follows: a) traffic, b) biomass burning, c) secondary inorganic aerosol, d) sea salt and e) dust. The reconstruction of the measured species by PMF was satisfactory, showing a strong correlation ($r^2 = 0.94$) with measured PM_{10} concentrations (Fig. 6).

The contributions of the individual sources for the days when the daily PM_{10} standard of 50 μg m^{-3} was exceeded were further investigated. The source contributions to the PM_{10} levels on days exceeding the EU limit were as follows: biomass burning (45%) > dust (25%) > traffic (23%) > SIA (6%) > sea salt (1%). In the first week of sampling, during which systematic exceedances were recorded, the contribution of biomass burning represented up to 70% of the measured PM_{10} concentrations, while the input from dust was greater than 85% on specific days of Saharan intrusions (February 19th and March 3rd). Moreover, as concerns the daytime-nighttime comparison, the investigation of the factor contributions to PM_{10} concentrations showed differences between daytime and nighttime, as shown in Fig. 7.

Source contributions to daytime PM_{10} were as follows: traffic (38%) > dust (26%) > biomass burning (14%) > SIA (11%) > sea salt (11%). The nighttime contributions were instead: biomass burning (30%) > traffic (26%) > dust (22%) > SIA (12%) > sea salt (10%). The differences in individual contributions by period were found to be statistically significant for biomass burning, traffic and dust.

As can be seen in Fig. 7, the contribution of biomass burning stands out during the night, while the other sources present variable contributions between the two periods of the day. The highest concentrations and contributions related to traffic and dust were recorded for the daytime period. These results are in line with previous findings by Cipoli et al. (2022), who reported morning peaks of PM linked to vehicle exhaust and non-exhaust emissions, as well as resuspension of road dust, exacerbated by construction activities. In the present study, the dust load spikes coincide with long-range transport from North Africa. Secondary aerosols showed a similar profile throughout the campaign for the diurnal and nocturnal periods, but with substantially greater contributions at night. Sea salt did not display significant differences between day and night, with very close contributions for both periods.

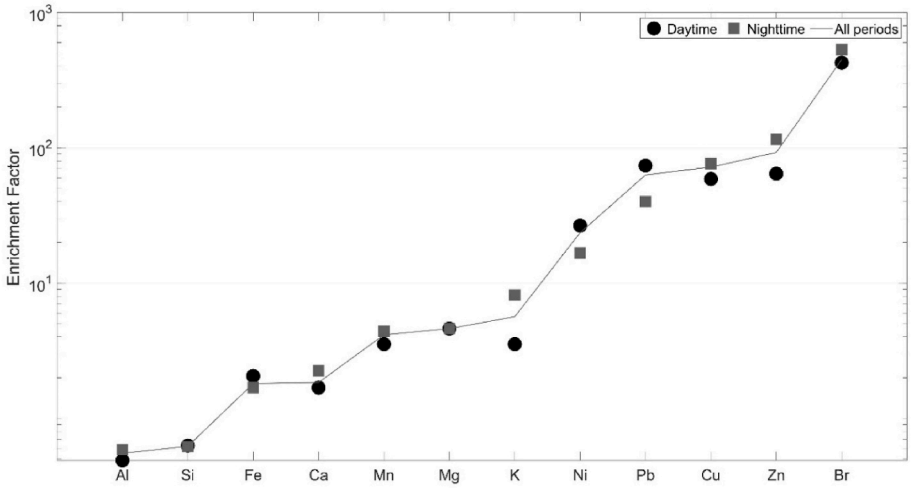

Fig. 4. Element enrichment factors using Al as a reference.

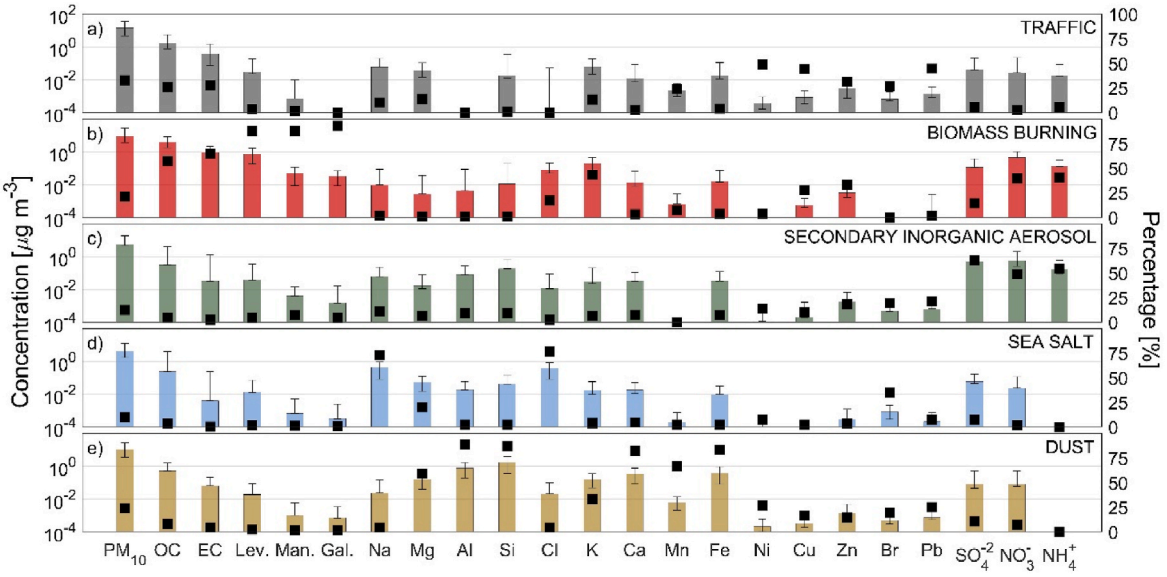

Fig. 5. Profiles for five sources identified using PMF (a) traffic, b) biomass burning, c) secondary inorganic aerosol, d) sea salt and e) dust). The bars show the mean concentration of the species, and the squares represent the percentage of each species in each factor. Bar error limits show the P5th and P95th for BS-DISP.

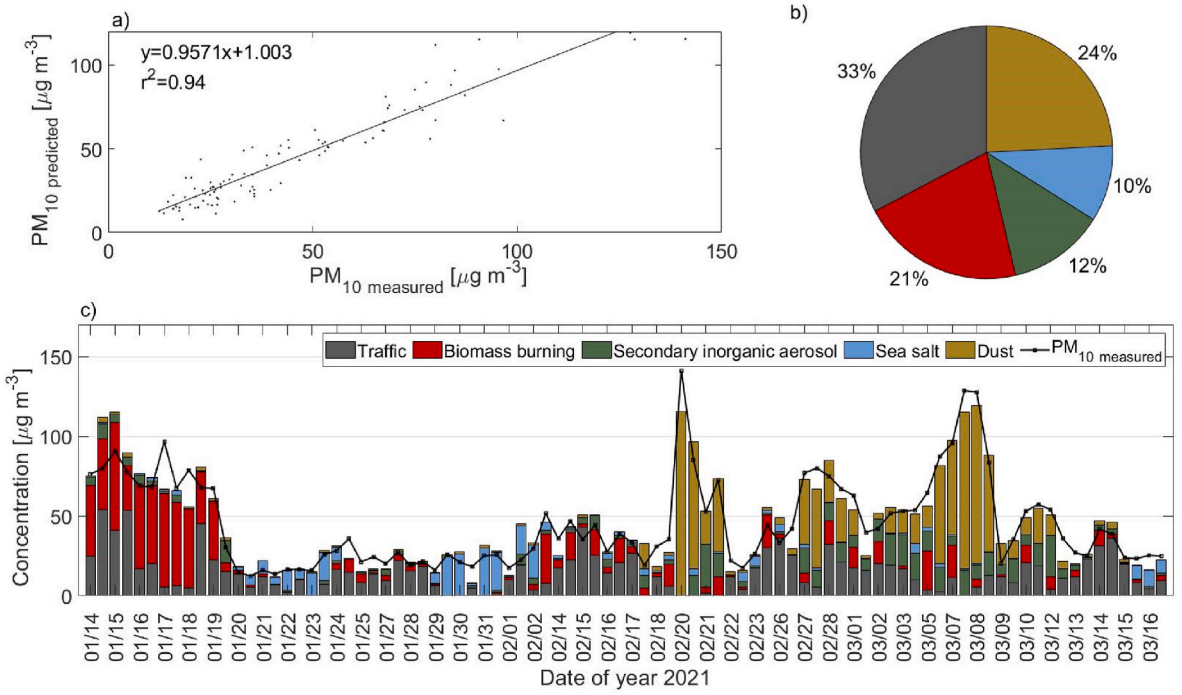

Fig. 6. a) Correlation between the values predicted by the PMF model and those measured by gravimetry, b) distribution of sources of PM_{10} and c) time series of source contributions for whole period.

3.4.1. *Traffic*

Factor analysis results identified the traffic source profile as the main contributor to daily PM_{10} concentrations (33%), with higher contributions during the daytime (Fig. S3). Globally, species concentrations obtained from the PMF for this source profile were, on average, 23% higher during the day. This difference probably reflects the weight of road traffic emissions, as the daytime period covered the morning peak and partially the afternoon rush hour. The species that most contributed to this factor were organic and elemental carbon, and Ni, Cu, Pb, Zn and Br. Similar species have been identified as vehicular emission markers (Begum et al., 2011; Crawford et al., 2007; Oduber et al., 2021; Saggu and Mittal, 2020). Trace metals such as Cu, Ni, and Zn are often originated from non-exhaust emissions, mainly related to brake and tyre wear (Thorpe and Harrison, 2008). Amato et al. (2016) and Pio et al. (2022) reported Cu/Fe ratios of 0.045 and 0.03, respectively, for non-exhaust emissions. The ratio of the present study (Cu/Fe = 0.029) is similar to the one documented by Pio et al. (2011). Furthermore, in a previous study, C.A. Alves et al. (2020) reported OC/EC ratios ranging from 3.19 to 6.95 when analysing wear particles from tyre-pavement interaction. The OC/EC ratio found for this profile was 3.57, indicating that an important fraction of the carbonaceous material in this source originates from non-exhaust emissions.

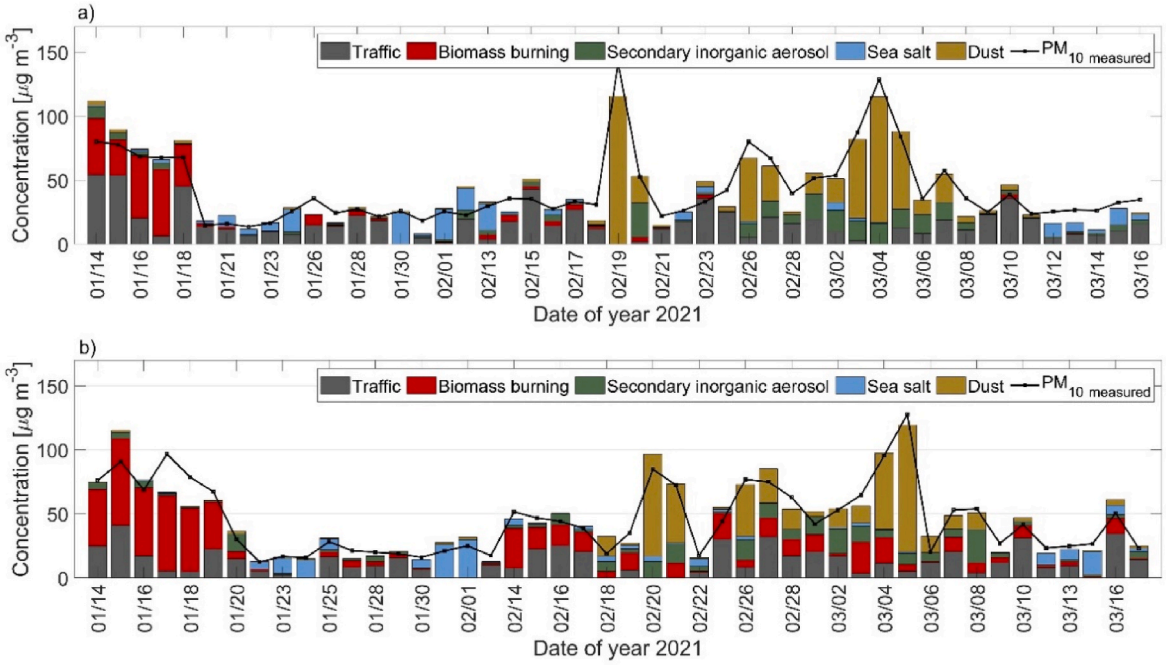

Fig. 7. Source contributions to PM_{10} from the PMF analysis for (a) daytime and (b) nighttime periods.

3.4.2. Biomass burning

The source identified as biomass burning was mainly resolved by the high concentrations of markers such as OC, levoglucosan, mannosan, galactosan, and K, and to a lesser extent by the presence of Cl, SO_4^{2-}, NO_3^- and NH_4^+. Anhydrosugars, such as levoglucosan, mannosan and galactosan, are major organic components of particles from biomass burning (Vicente and Alves, 2018). Increases of 63% in species concentrations were found at night compared to daytime, indicating a more frequent and intense presence of this source after sunset. As expected, this factor was characterised by high mass contributions (11.7%) from levoglucosan during nighttime, while for the daytime period a share of 5% was registered. Gonçalves et al. (2010) reported levoglucosan-mannosan ratios in the range from 10.4 to 34.9 for hardwood burning. In the present study, a levoglucosan/mannosan ratio of 13.8 was obtained, suggesting the predominant use of hardwoods, such as oak, chestnut and poplar, which are biofuels commonly consumed in Bragança, mainly for residential heating, but also for cooking. The mass contribution of carbonaceous material to this profile was dominant (55% OC and 15% EC). OC/levoglucosan ratios similar to that of the present study (5.1) were reported for Porto (5.4) and Coimbra (5.3), both cities in northern Portugal (Pio et al., 2020, 2022). NO_3^- accounted for 8% of the source mass. Although NO_3^- is not a direct tracer of residential biomass burning emissions (Alves et al., 2011), the NO_3^-/levoglucosan ratio (0.7) of the current profile coincide with the value obtained by Amato et al. (2016) for the same source profile after applying PMF to a database of the city of Porto. In a study carried out in Coimbra, Pio et al. (2022) documented a higher ratio of 2.3 for this profile, suggesting source contamination by secondary nitrates formed by other emitting sources. Especially at night, lower temperatures and wind speeds, concurrently with stronger emissions from domestic heating and cooking in the winter months, contribute to the increased share of biomass burning in PM_{10} concentrations.

3.4.3. Secondary inorganic aerosol

The factor characterised as "secondary inorganic aerosol" was highly loaded with NO_3^- (29%), SO_4^{2-} (22%) and NH_4^+ (12%). Concentrations of NO_3^-, SO_4^{2-} and NH_4^+ during the night were found to be 14%, 9% and 17% higher compared to the daytime, respectively. Higher concentrations of NO_3^- were concomitant with higher levels of NOx at night (Fig. S1). The high correlations between NH_4^+ and NO_3^- ($r^2 = 0.95$) suggest that NH_3 was neutralised by sulphuric acid to form $(NH_4)_2SO_4$, but NH_3 in excess have reacted with HNO_3 to yield NH_4NO_3. The higher NO_3^- and NH_4^+ loads during nighttime can be attributed to thermal stability of NH_4NO_3 at low temperature and/or heterogeneous formation of NO_3^- (via hydrolysis of N_2O_5) under high humidity conditions. The evaporative loss of NH_4NO_3 at higher temperatures has been suggested as an alternate explanation for the lower levels during daytime (Ram and Sarin, 2011). Likewise, as the air cools at night, the haze can turn to fog, enhancing the atmospheric liquid water content by orders of magnitude and hence the importance of SO_2 aqueous-phase oxidation pathways (Wang et al., 2020). Significant correlations were found between SO_4^{2-} and major constituents of dust (Tables S6–S7). It has been reported that, on the dust surface, heterogeneous drivers, such as transition metal constituents, and water-soluble ions, are more efficient than surface adsorbed oxidants (e.g., H_2O_2, NO_2, O_3) in the conversion of SO_2 to particulate sulphate, especially during nighttime (Wang et al., 2022). The results indicated that SIA is associated with local anthropic activities, especially traffic, and biomass burning, but also with long-range transport.

3.4.4. Sea salt

The contribution of sea salt was identified by the high abundances of Cl (80%) and Na (78%), and lower proportions of Br (27%) and Mg (22%). This is in agreement with other "marine aerosol" source profiles (Almeida et al., 2005; Amato et al., 2016; Waked et al., 2014). The Cl/Na ratios (1.7 nighttime, 0.95 daytime) were close to those reported for seawater (1.8), while the Mg/Na ratios (0.67 nighttime, 0.72 daytime) were higher than the value (0.14) documented for sea-salt particles (Mouri et al., 1993; Seinfeld and Pandis, 2006). This could be explained by the large contribution of magnesium from crustal origin.

The overall contribution of this factor to PM_{10} (10%) is slightly higher than the 6% contribution by sea salt estimated by mass balance. Pio et al. (2022) measured PM_{10} simultaneously at a roadside (RS) and an urban background (UB) location in Coimbra, Portugal. On average, fresh sea salt accounted for 6% and 9% at RS when estimated by PMF or mass balance, respectively, while the corresponding values at UB were 10% and 11%. In a traffic-impacted site in the coastal city of Porto, sea salt represented 16% of the PM_{10} concentrations, according to estimates

by both methodologies (Amato et al., 2016).

3.4.5. Dust

The dust source was represented by high contributions of Al, Si, Mg, Ca, Mn, and Fe (Fig. S4). These elements have been associated with road dust resuspension, and desert dust intrusions (Fujiwara et al., 2011; Jaeckels et al., 2007; Taghvaee et al., 2018), in line with the composition of the upper earth's crust (Chen et al., 2016). Alves et al. (2018) analysed road dust from five main roads of a large city in Portugal and found that crustal elements such as Al, Ca and Fe were the most abundant in PM_{10}. All these elements had high contributions to this factor: Al (85%), Ca (80%) and Fe (75%). The high levels of Ca may, in part, be originated from construction activities (Crilley et al., 2017), while the abundance of Fe may be somewhat related to brake and tyre wear particles that are deposited on the roads and then resuspended by the action of the wind or passing vehicles (Gietl et al., 2010; Grigoratos and Martini, 2015; Alves et al., 2018). Several construction activities were being undertaken during the sampling period, which may have contributed to the Ca levels in this factor. All the main elements contributing to this source were characterised as having a mostly crustal origin (enrichment factor <10, Fig. 2). Significant contributions to the increase in concentrations of the elements that make up this source are related to long-range dust transport events (Fernández et al., 2019). During the study period, approximately 14% of the samples were contaminated with dust intrusions from the Sahara (see more details in the next section). Dust accounted for 66%, 65%, 64%, 59% and 38% of the total concentrations of Si, Al, Ca, Fe, and Mn, respectively. Dust contributions to PM_{10} between daytime and nighttime were close (26% and 22%, respectively). However, higher contributions at night were observed during dust outbreaks. Since the mixing height decreases very rapidly as the sun sets, and the nightly decrease in wind speed diminishes even more the nocturnal atmospheric dispersion capacity, higher dust concentrations are observed during dark hours. During the day, in addition to dust intrusions, non-exhaust emissions from road traffic, construction activities and soil dust resuspension also contributed to this source factor.

3.4.6. Location of the sources

The daily contributions from sources to PM_{10} concentrations as a function of wind speed and direction (polar coordinates) is shown in Fig. 8, allowing a graphical inference of the origin of the emissions that affected the receptor site. The graphs reveal that contributions from different sources are associated with different wind directions, although there is overlapping of contributions for similar quadrants. The highest PM_{10} concentrations from biomass burning, whether for daytime or nighttime, were located in the first quadrant, and associated with low wind speeds (<3 m s^{-1}), suggesting contributions very close to the receptor site (Yu et al., 2004). In this sector, old residential neighbourhoods of the city are located, which are characterised by more inefficient domestic heating devices (e.g., open fireplaces). The traffic polar plot shows high concentrations for all quadrants, reflecting the location of the monitoring site, which is surrounded by avenues around its perimeter. In addition, traffic daytime contributions >15 μg m^{-3} were registered for lower wind speeds with southwest to northwest directions, where rather more congested downtown traffic takes place (Cipoli et al., 2022). At night, higher contributions were also observed for the east and southeast directions, reflecting late afternoon homecoming traffic emissions due to commuting to the outskirts of the city and neighbouring municipalities after the working day. The contribution of SIA was in line with those from traffic, biomass burning, and dust, suggesting the formation of precursors in sectors with greater inputs from these sources. Sea salt showed higher concentrations for higher wind speeds coming from the southwest to west directions, pointing towards aerosols transported from the Atlantic coast. Higher dust contributions were associated with winds from north to south quadrants, in accordance with the long-range transport of dust plumes crossing the Iberian Peninsula. Twelve days that had dust concentrations above the 90th percentile (75 μg m^{-3}) were analysed by backward trajectories to check possible Saharan dust intrusions. However, only 3 days were clearly affected by pure long-range transport from north Africa (Fig. S5). The other nine days may have been influenced by mixed aerosol regimes. An aerosol regime containing only mineral dust particles is less frequent because, during the winter months, the Harmattan carries Saharan dust particles at lower altitudes, promoting mixing with marine aerosol (Gutleben et al., 2022).

3.5. Ecotoxicological assessment of PM_{10} samples

The ecotoxicity of 34 samples of PM_{10}, representing two different periods (1st group - Jan 14th to 21st and 2nd group - Feb 25th to Mar 05th) is shown in Fig. 9. In 76% of the samples, the percentage of inhibition was above 50%, suggesting that the chemical composition of the samples had a toxic effect. TU_{50} variations in the range from 0.3 to 27.5 were observed. According to the data, 18% of the samples were considered 'very toxic', 53% 'toxic' and 29% 'non-toxic'. When analysing the contributions of each source and their correlation with the toxicity, a significant correlation was observed only for biomass burning ($r^2 = 0.87$ and $p < 0.05$). Furthermore, significant correlations were found for specific PM_{10}-bound constituents: OC ($r^2 = 0.65$), EC ($r^2 = 0.64$), Zn ($r^2 = 0.68$), K ($r^2 = 0.54$), levoglucosan ($r^2 = 0.86$), mannosan ($r^2 = 0.81$), galactosan (0.84), NO_3^- ($r^2 = 0.45$) and NH_4^+ ($r^2 = 0.48$). These constituents were part of the biomass source profile, reinforcing the role of this source in the toxicity of the samples. The 1st group of samples showed higher toxicity than those from the 2nd group, possibly due to the strength of the biomass burning source, especially during the nighttime (bars with white stripes), when the toxicity was 38% higher than that of daytime samples. These results are in agreement with those of Aammi et al. (2017), who attributed the toxicity of samples in the cold season to anthropogenic activities (residential biomass combustion) and seasonal effects (inversion layers and atmospheric stability).

Previous studies have highlighted differences in toxicity values as a function of sampling sites and sources contributing to PM. For instance, Vicente et al. (2021) found TU_{50} values ranging from 1.4 (toxic) to 103 (very toxic) for PM samples collected inside homes when evaluating biomass combustion appliances (fireplace and wood stove). As observed by Yang et al. (2016), the toxicity of heavy metals (Zn, Cu, Cd, Cr) as a function of the luminescence inhibition rate increased over the reaction time, while the organic compounds maintained similar reaction times. Lower toxicity values (1.5–3.1) for PM_{10} samples were reported by Romano et al. (2020), who found significant positive correlations with the main species emitted by combustion sources (OC, EC, K). The increased toxicity of PM-bound organic compounds from biomass burning was also documented by Sainnokhoi et al. (2022). Non-toxic samples were observed mainly for the 2nd group, for which biomass burning had less expressive contributions. During this period, Saharan dust intrusions were recorded, even though, no significant correlations were found with crustal elements and levels of toxicity. The results of the present study indicate that, even with lower contributions from biomass burning, toxicity can still be induced.

4. Conclusions

For the first time in Bragança, a winter PM_{10} sampling campaign was carried out, with segregation between day and night, in order to assign the sources that contribute to the observed levels. The daily concentrations of $PM_{2.5}$ and PM_{10} were, in 24% and 20% of the campaign days, respectively, higher than the limit values established by the Directive 2008/50/EC. Positive matrix factorisation analysis was able to discriminate 5 main sources: traffic (33%), biomass burning (21%), secondary inorganic aerosols (12%), sea salt (10%) and dust (24%). During periods of exceedances of the daily PM_{10} limit value, Saharan dust intrusions and biomass burning for residential heating were identified as the main sources. In the coldest period, the contribution of

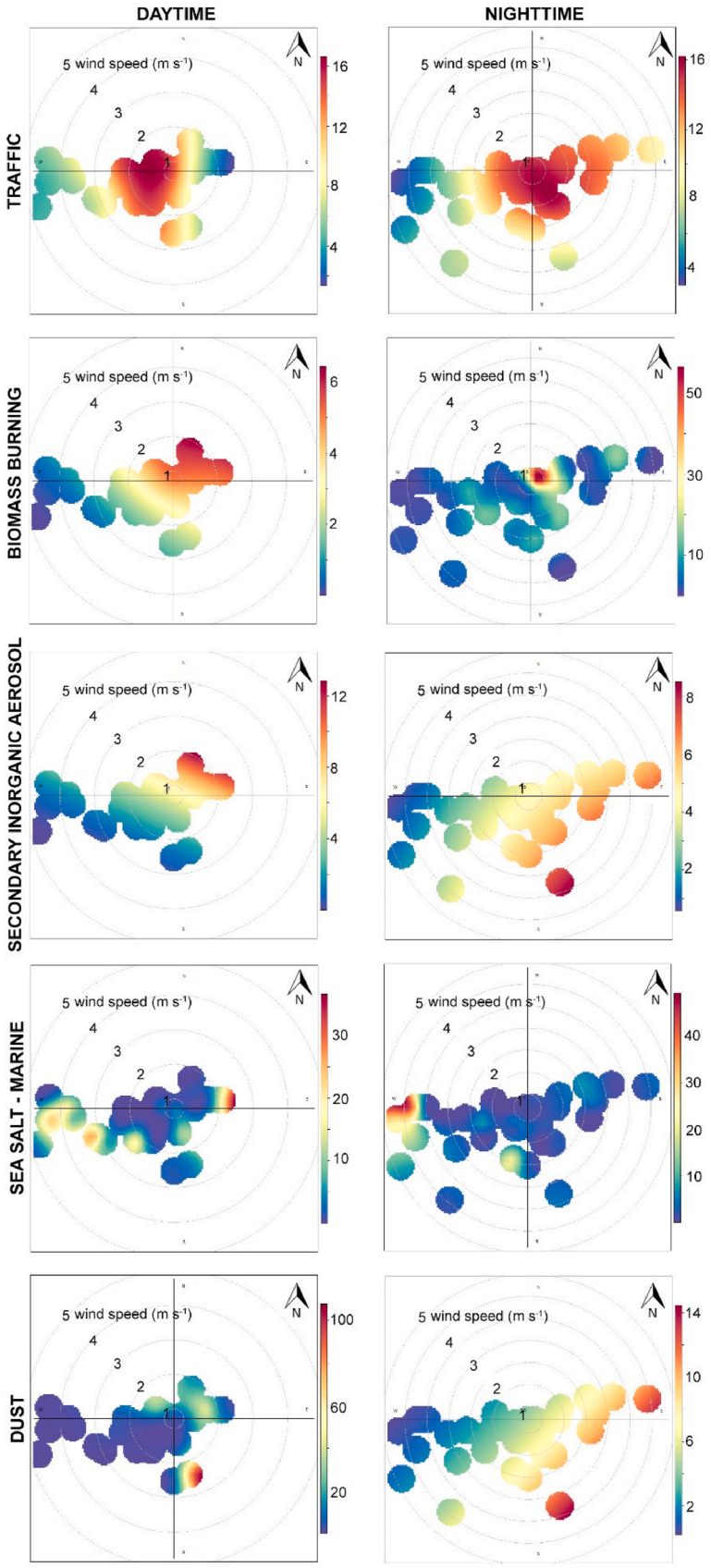

Fig. 8. Polar plots of PM_{10} source concentrations (μg m^{-3}) as a function of wind speed and direction. The radial dimension for each polar plot indicates wind speed (m s^{-1}).

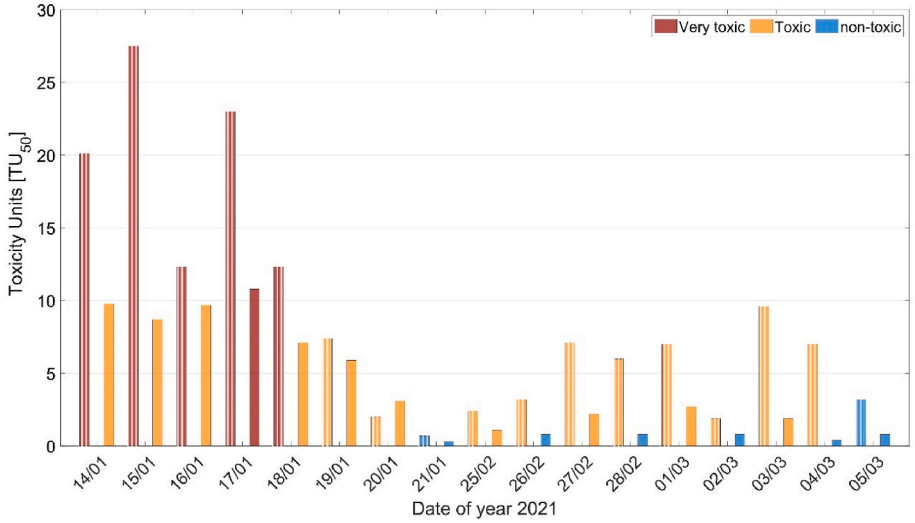

Fig. 9. Toxicity Units (TU50) obtained for the PM_{10} samples collected during the nighttime and daytime. The nighttime is identified by bars with white stripes.

biomass burning accounted for up to 70% of the PM_{10} concentrations. Furthermore, the results obtained from the chemical mass closure were consistent and coherent with the results of the PMF, providing confidence to the assignment of sources made.

Day-night differences for the observed sources were found to be significant. Traffic and dust contributed most during the day, due to exhaust and non-exhaust emissions and dust intrusions. The nocturnal samples showed a dominance of the biomass burning source, due to residential heating and cooking appliances. In addition, the bioluminescence inhibition assay pointed to burning of biomass as the most harmful source, showing that the toxicological responses are related to the chemical composition of the particles. Findings of this study can support the development of effective mitigation measures. Based on the source apportionment results, it can be inferred that the sole reduction of biomass burning emissions would represent an important action to lower the PM_{10} mass concentrations and their toxic effects. With inflation and high energy prices continuing to mark the political agenda of the European Union, an intensification in the consumption of biomass is to be expected, which is why it is necessary to take urgent measures to reduce emissions from this combustion source. National replacement schemes for old stoves, public incentives for investment in new appliances, regular on-site inspections, advanced stove/boiler ecolabels, and public information campaigns are possible measures to adopt.

Declaration of competing interest

The authors declare that they have no known competing financial interests or personal relationships that could have appeared to influence the work reported in this paper.

Data availability

Data will be made available on request.

Acknowledgments

Yago A. Cipoli acknowledges the Portuguese Foundation of Science and Technology (FCT) for the PhD scholarship (SFRH/BD/04992/2021). The authors are grateful to FCT for its financial support through national funds FCT/MCTES (PIDDAC) to CIMO (UIDB/00690/2020 and UIDP/00690/2020), SusTEC (LA/P/0007/2020) and CESAM (UIDP/50017/2020, UIDB/50017/2020 and LAP/0094/2020). We are grateful for the collaboration of Prof. Franco Lucarelli, from the University of Florence, in the analysis of elements by PIXE. The support from the RADIATE project 21002436-ST is recognised as well. We are also grateful for the support of Doctor Cátia Gonçalves in the analysis of anhydrosugars at CESAM.

Appendix A. Supplementary data

Supplementary data to this article can be found online at https://doi.org/10.1016/j.atmosenv.2023.119771.

References

Aammi, S., Karaca, F., Petek, M., 2017. A toxicological and genotoxicological indexing study of ambient aerosols ($PM_{2.5-10}$) using in vitro bioassays. Chemosphere 174, 490–498. https://doi.org/10.1016/J.CHEMOSPHERE.2017.01.141.

Almeida, S.M., Pio, C.A., Freitas, M.C., Reis, M.A., Trancoso, M.A., 2005. Source apportionment of fine and coarse particulate matter in a sub-urban area at the Western European Coast. Atmos. Environ. 39, 127–3138. https://doi.org/10.1016/J.ATMOSENV.2005.01.048.

Alves, C.A., Vicente, A.M.P., Calvo, A.I., Baumgardner, D., Amato, F., Querol, X., Pio, C., Gustafsson, M., 2020. Physical and chemical properties of non-exhaust particles generated from wear between pavements and tyres. Atmos. Environ. 224, 117252 https://doi.org/10.1016/J.ATMOSENV.2019.117252.

Alves, C., Gonçalves, C., Fernandes, A.P., Tarelho, L., Pio, C., 2011. Fireplace and woodstove fine particle emissions from combustion of western Mediterranean wood types. Atmos. Res. 101, 692–700. https://doi.org/10.1016/J.ATMOSRES.2011.04.015.

Alves, C.A., Evtyugina, M., Vicente, A.M.P., Vicente, E.D., Nunes, T.V., Silva, P.M.A., Duarte, M.A.C., Pio, C.A., Amato, F., Querol, X., 2018. Chemical profiling of PM_{10} from urban road dust. Sci. Total Environ. 634, 41–51. https://doi.org/10.1016/J.SCITOTENV.2018.03.338.

Alves, C.A., Vicente, E.D., Vicente, A.M.P., Rienda, I.C., Tomé, M., Querol, X., Amato, F., 2020. Loadings, chemical patterns and risks of inhalable road dust particles in an Atlantic city in the north of Portugal. Sci. Total Environ. 737, 139596 https://doi.org/10.1016/J.SCITOTENV.2020.139596.

Amato, F., Alastuey, A., Karanasiou, A., Lucarelli, F., Nava, S., Calzolai, G., Severi, M., Becagli, S., Gianelle, V.L., Colombi, C., Alves, C., Custódio, D., Nunes, T., Cerqueira, M., Pio, C., Eleftheriadis, K., Diapouli, E., Reche, C., Minguillón, M.C., Manousakas, M.I., Maggos, T., Vratolis, S., Harrison, R.M., Querol, X., 2016. AIRUSE-LIFE+: a harmonized PM speciation and source apportionment in five southern European cities. Atmos. Chem. Phys. 16, 3289–3309. https://doi.org/10.5194/ACP-16-3289-2016.

Begum, B.A., Biswas, S.K., Hopke, P.K., 2011. Key issues in controlling air pollutants in Dhaka, Bangladesh. Atmos. Environ. 45, 7705–7713. https://doi.org/10.1016/J.ATMOSENV.2010.10.022.

Behera, S.N., Sharma, M., Aneja, V.P., Balasubramanian, R., 2013. Ammonia in the atmosphere: a review on emission sources, atmospheric chemistry and deposition on terrestrial bodies. Environ. Sci. Pollut. Res. 20, 8092–8131. https://doi.org/10.1007/S11356-013-2051-9/TABLES/16.

Belis, C.A., Karagulian, F., Larsen, B.R., Hopke, P.K., 2013. Critical review and meta-analysis of ambient particulate matter source apportionment using receptor models in Europe. Atmos. Environ. 69, 94–108. https://doi.org/10.1016/J.ATMOSENV.2012.11.009.

Biegalski, S.R., Landsberger, S., Hoff, R.M., 1998. Source-receptor modeling using trace metals in aerosols collected at three rural Canadian great lakes sampling stations.

J. Air Waste Manage. Assoc. 48, 227–237. https://doi.org/10.1080/10473289.1998.10463680.
Brines, M., Dall'Osto, M., Amato, F., Minguillón, M.C., Karanasiou, A., Grimalt, J.O., Alastuey, A., Querol, X., van Drooge, B.L., 2019. Source apportionment of urban PM_1 in Barcelona during SAPUSS using organic and inorganic components. Environ. Sci. Pollut. Res. 26, 32114–32127. https://doi.org/10.1007/S11356-019-06199-3/FIGURES/3.
Brook, R.D., Rajagopalan, S., Pope, C.A., Brook, J.R., Bhatnagar, A., Diez-Roux, A.V., Holguin, F., Hong, Y., Luepker, R.V., Mittleman, M.A., Peters, A., Siscovick, D., Smith, S.C., Whitsel, L., Kaufman, J.D., 2010. Particulate matter air pollution and cardiovascular disease. Circulation 121, 2331–2378. https://doi.org/10.1161/CIR.0B013E3181DBECE1.
Calzolai, G., Chiari, M., Lucarelli, F., Nava, S., Taccetti, F., Becagli, S., Frosini, D., Traversi, R., Udisti, R., 2014. PIXE–PIGE analysis of size-segregated aerosol samples from remote areas. Nucl. Instrum. Methods Phys. Res. Sect. B Beam Interact. Mater. Atoms 318, 125–129. https://doi.org/10.1016/J.NIMB.2013.05.097.
Calzolai, G., Nava, S., Lucarelli, F., Chiari, M., Giannoni, M., Becagli, S., Traversi, R., Marconi, M., Frosini, D., Severi, M., Udisti, R., Di Sarra, A., Pace, G., Meloni, D., Bommarito, C., Monteleone, F., Anello, F., Sferlazzo, D.M., 2015. Characterization of PM_{10} sources in the central Mediterranean. Atmos. Chem. Phys. 15, 13939–13955. https://doi.org/10.5194/ACP-15-13939-2015.
Carslaw, D.C., Ropkins, K., 2012. Openair — an R package for air quality data analysis. Environ. Model. Software 27 (28), 52–61. https://doi.org/10.1016/J.ENVSOFT.2011.09.008.
Cesari, D., De Benedetto, G.E., Bonasoni, P., Busetto, M., Dinoi, A., Merico, E., Chirizzi, D., Cristofanelli, P., Donateo, A., Grasso, F.M., Marinoni, A., Pennetta, A., Contini, D., 2018. Seasonal variability of $PM_{2.5}$ and PM_{10} composition and sources in an urban background site in Southern Italy. Sci. Total Environ. 612, 202–213. https://doi.org/10.1016/J.SCITOTENV.2017.08.230.
Chatoutsidou, S.E., Lazaridis, M., 2022. Mass concentrations and elemental analysis of $PM_{2.5}$ and PM_{10} in a coastal Mediterranean site: a holistic approach to identify contributing sources and varying factors. Sci. Total Environ. 838, 155980 https://doi.org/10.1016/J.SCITOTENV.2022.155980.
Chen, J., Hoek, G., 2020. Long-term exposure to PM and all-cause and cause-specific mortality: a systematic review and meta-analysis. Environ. Int. 143, 105974 https://doi.org/10.1016/J.ENVINT.2020.105974.
Chen, Yuan, Schleicher, N., Cen, K., Liu, X., Yu, Y., Zibat, V., Dietze, V., Fricker, M., Kaminski, U., Chen, Yizhen, Chai, F., Norra, S., 2016. Evaluation of impact factors on $PM_{2.5}$ based on long-term chemical components analyses in the megacity Beijing, China. Chemosphere 155, 234–242. https://doi.org/10.1016/J.CHEMOSPHERE.2016.04.052.
Chow, J.C., Lowenthal, D.H., Chen, L.W.A., Wang, X., Watson, J.G., 2015. Mass reconstruction methods for $PM_{2.5}$: a review. Air Qual. Atmos. Heal. 8, 243–263. https://doi.org/10.1007/S11869-015-0338-3/TABLES/4.
Cipoli, Y.A., Targino, A.C., Krecl, P., Furst, L.C., Alves, C., dos, A., Feliciano, M., 2022. Ambient concentrations and dosimetry of inhaled size-segregated particulate matter during periods of low urban mobility in Bragança. Portugal. Atmos. Pollut. Res. 13, 101512 https://doi.org/10.1016/J.APR.2022.101512.
Contini, D., Cesari, D., Genga, A., Siciliano, M., Ielpo, P., Guascito, M.R., Conte, M., 2014. Source apportionment of size-segregated atmospheric particles based on the major water-soluble components in Lecce (Italy). Sci. Total Environ. 472, 248–261. https://doi.org/10.1016/J.SCITOTENV.2013.10.127.
Crawford, J., Chambers, S., Cohen, D.D., Dyer, L., Wang, T., Zahorowski, W., 2007. Receptor modelling using positive matrix factorisation, back trajectories and radon-222. Atmos. Environ. 41, 6823–6837. https://doi.org/10.1016/J.ATMOSENV.2007.04.048.
Crilley, L.R., Lucarelli, F., Bloss, W.J., Harrison, R.M., Beddows, D.C., Calzolai, G., Nava, S., Valli, G., Bernardoni, V., Vecchi, R., 2017. Source apportionment of fine and coarse particles at a roadside and urban background site in London during the 2012 summer ClearfLo campaign. Environ. Pollut. 220, 766–778. https://doi.org/10.1016/J.ENVPOL.2016.06.002.
de Miranda, R.M., de Fatima Andrade, M., Dutra Ribeiro, F.N., Mendonça Francisco, K.J., Pérez-Martínez, P.J., 2018. Source apportionment of fine particulate matter by positive matrix factorization in the metropolitan area of São Paulo, Brazil. J. Clean. Prod. 202, 253–263. https://doi.org/10.1016/J.JCLEPRO.2018.08.100.
EEA, 2022. Air Quality in Europe - 2022 Report — European Environment Agency. https://www.eea.europa.eu/publications/status-of-air-quality-in-Europe-2022/europes-air-quality-status-2022.
Fernández, A.J., Sicard, M., Costa, M.J., Guerrero-Rascado, J.L., Gómez-Amo, J.L., Molero, F., Barragán, R., Basart, S., Bortoli, D., Bedoya-Velásquez, A.E., Utrillas, M. P., Salvador, P., Granados-Muñoz, M.J., Potes, M., Ortiz-Amezcua, P., Martínez-Lozano, J.A., Artíñano, B., Muñoz-Porcar, C., Salgado, R., Román, R., Rocadenbosch, F., Salgueiro, V., Benavent-Oltra, J.A., Rodríguez-Gómez, A., Alados-Arboledas, L., Comerón, A., Pujadas, M., 2019. Extreme, wintertime Saharan dust intrusion in the Iberian Peninsula: lidar monitoring and evaluation of dust forecast models during the February 2017 event. Atmos. Res. 228, 223–241. https://doi.org/10.1016/J.ATMOSRES.2019.06.007.
Fujiwara, F.G., Gómez, D.R., Dawidowski, L., Perelman, P., Faggi, A., 2011. Metals associated with airborne particulate matter in road dust and tree bark collected in a megacity (Buenos Aires, Argentina). Ecol. Indicat. 11, 240–247. https://doi.org/10.1016/J.ECOLIND.2010.04.007.
Fuzzi, S., Baltensperger, U., Carslaw, K., Decesari, S., Denier Van Der Gon, H., Facchini, M.C., Fowler, D., Koren, I., Langford, B., Lohmann, U., Nemitz, E., Pandis, S., Riipinen, I., Rudich, Y., Schaap, M., Slowik, J.G., Spracklen, D.V., Vignati, E., Wild, M., Williams, M., Gilardoni, S., 2015. Particulate matter, air quality and climate: lessons learned and future needs. Atmos. Chem. Phys. 15, 8217–8299. https://doi.org/10.5194/ACP-15-8217-2015.
Galindo, N., Yubero, E., 2017. Day-night variability of water-soluble ions in PM_{10} samples collected at a traffic site in southeastern Spain. Environ. Sci. Pollut. Res. 24, 805–812. https://doi.org/10.1007/S11356-016-7836-1/FIGURES/5.
Gao, L., Li, Z., Zou, Y., Yin, S., Peng, P., Shao, Y., Liang, X., 2020. A high-performance aqueous zinc-bromine static battery. iScience 23, 101348. https://doi.org/10.1016/J.ISCI.2020.101348.
Ghosh, R., Causey, K., Burkart, K., Wozniak, S., Cohen, A., Brauer, M., 2021. Correction: ambient and household $PM_{2.5}$ pollution and adverse perinatal outcomes: a meta-regression and analysis of attributable global burden for 204 countries and territories. PLoS Med. 18, e1003852 https://doi.org/10.1371/JOURNAL.PMED.1003852.
Gietl, J.K., Lawrence, R., Thorpe, A.J., Harrison, R.M., 2010. Identification of brake wear particles and derivation of a quantitative tracer for brake dust at a major road. Atmos. Environ. 44, 141–146. https://doi.org/10.1016/J.ATMOSENV.2009.10.016.
Gonçalves, C., Alves, C., Evtyugina, M., Mirante, F., Pio, C., Caseiro, A., Schmidl, C., Bauer, H., Carvalho, F., 2010. Characterisation of PM_{10} emissions from woodstove combustion of common woods grown in Portugal. Atmos. Environ. 44, 4474–4480. https://doi.org/10.1016/J.ATMOSENV.2010.07.026.
Gonçalves, C., Rienda, I.C., Pina, N., Gama, C., Nunes, T., Tchepel, O., Alves, C., 2021. PM_{10}-Bound sugars: chemical composition, sources and seasonal variations. Atmos 12, 194. https://doi.org/10.3390/ATMOS12020194.
Grigoratos, T., Martini, G., 2015. Brake wear particle emissions: a review. Environ. Sci. Pollut. Res. 22, 2491–2504. https://doi.org/10.1007/S11356-014-3696-8/TABLES/5.
Gutleben, M., Groß, S., Heske, C., Wirth, M., 2022. Wintertime Saharan dust transport towards the Caribbean: an airborne lidar case study during EUREC4A. Atmos. Chem. Phys. 22, 7319–7330. https://doi.org/10.5194/ACP-22-7319-2022.
Han, B., Zhang, R., Yang, W., Bai, Z., Ma, Z., Zhang, W., 2016. Heavy haze episodes in Beijing during January 2013: inorganic ion chemistry and source analysis using highly time-resolved measurements from an urban site. Sci. Total Environ. 544, 319–329. https://doi.org/10.1016/J.SCITOTENV.2015.10.053.
Hannan, M.A., Hoque, M.M., Mohamed, A., Ayob, A., 2017. Review of energy storage systems for electric vehicle applications: issues and challenges. Renew. Sustain. Energy Rev. 69, 771–789. https://doi.org/10.1016/J.RSER.2016.11.171.
Hans Wedepohl, K., 1995. The composition of the continental crust. Geochem. Cosmochim. Acta 59, 1217–1232. https://doi.org/10.1016/0016-7037(95)00038-2.
Hopke, P.K., Dai, Q., Li, L., Feng, Y., 2020. Global review of recent source apportionments for airborne particulate matter. Sci. Total Environ. 740, 140091 https://doi.org/10.1016/J.SCITOTENV.2020.140091.
Jaeckels, J.M., Bae, M.S., Schauer, J.J., 2007. Positive matrix factorisation (PMF) analysis of molecular marker measurements to quantify the sources of organic aerosols. Environ. Sci. Technol. 41, 5763–5769. https://doi.org/10.1021/ES062536B/SUPPL_FILE/ES062536BSI20070602_090958.PDF.
Kanakidou, M., Seinfeld, J.H., Pandis, S.N., Barnes, I., Dentener, F.J., Facchini, M.C., Van Dingenen, R., Ervens, B., Nenes, A., Nielsen, C.J., Swietlicki, E., Putaud, J.P., Balkanski, Y., Fuzzi, S., Horth, J., Moortgat, G.K., Winterhalter, R., Myhre, C.E.L., Tsigaridis, K., Vignati, E., Stephanou, E.G., Wilson, J., 2005. Organic aerosol and global climate modelling: a review. Atmos. Chem. Phys. 5, 1053–1123. https://doi.org/10.5194/ACP-5-1053-2005.
Khodeir, M., Shamy, M., Alghamdi, M., Zhong, M., Sun, H., Costa, M., Chen, L.C., Maciejczyk, P., 2012. Source apportionment and elemental composition of $PM_{2.5}$ and PM_{10} in jeddah city, Saudi arabia. Atmos. Pollut. Res. 3, 331–340. https://doi.org/10.5094/APR.2012.037.
Kováts, N., Ács, A., Kovács, A., Ferincz, Á., Turóczi, B., Gelencsér, A., 2012. Direct contact test for estimating the ecotoxicity of aerosol samples. Environ. Toxicol. Pharmacol. 33, 284–287. https://doi.org/10.1016/J.ETAP.2011.12.021.
Kováts, N., Horváth, E., 2016. Bioluminescence-based assays for assessing eco- and genotoxicity of airborne emissions. Luminescence 31, 918–923. https://doi.org/10.1002/BIO.3102.
Lucarelli, F., Calzolai, G., Chiari, M., Giardi, F., Czelusniak, C., Nava, S., 2020. Hourly elemental composition and source identification by positive matrix factorization (PMF) of fine and coarse particulate matter in the high polluted industrial area of taranto (Italy), 2020 Atmos 11, 419. https://doi.org/10.3390/ATMOS11040419. Page 419 11.
Lucarelli, F., Calzolai, G., Chiari, M., Nava, S., Carraresi, L., 2018. Study of atmospheric aerosols by IBA techniques: the LABEC experience. Nucl. Instrum. Methods B. 417, 121–127. https://doi.org/10.1016/j.nimb.2017.07.034.
Manousakas, M., Papaefthymiou, H., Diapouli, E., Migliori, A., Karydas, A.G., Bogdanovic-Radovic, I., Eleftheriadis, K., 2017. Assessment of $PM_{2.5}$ sources and their corresponding level of uncertainty in a coastal urban area using EPA PMF 5.0 enhanced diagnostics. Sci. Total Environ. 574, 155–164. https://doi.org/10.1016/J.SCITOTENV.2016.09.047.
Miller, A.J., Raduma, D.M., George, L.A., Fry, J.L., 2019. Source apportionment of trace elements and black carbon in an urban industrial area (Portland, Oregon). Atmos. Pollut. Res. 10, 784–794. https://doi.org/10.1016/J.APR.2018.12.006.
Mouri, H., Okada, K., Shigehara, K., 1993. Variation of Mg, S, K and Ca contents in individual sea-salt particles. Tellus B 45, 80–85. https://doi.org/10.1034/J.1600-0889.1993.00007.X.
Nava, S., Calzolai, G., Chiari, M., Giannoni, M., Giardi, F., Becagli, S., Severi, M., Traversi, R., Lucarelli, F., 2020. Source apportionment of PM2.5 in florence (Italy) by PMF analysis of aerosol composition records, 2020 Atmos 11, 484. https://doi.org/10.3390/ATMOS11050484. Page 484 11.
Nayebare, S.R., Aburizaiza, O.S., Siddique, A., Carpenter, D.O., Hussain, M.M., Zeb, J., Aburiziza, A.J., Khwaja, H.A., 2018. Ambient air quality in the holy city of Makkah:

a source apportionment with elemental enrichment factors (EFs) and factor analysis (PMF). Environ. Pollut. 243, 1791–1801. https://doi.org/10.1016/J.ENVPOL.2018.09.086.

Norris, G., Duvall, R., 2014. EPA Positive Matrix Factorisation 5.0 Fundamentals and User Guide. https://www.epa.gov/sites/default/files/2015-02/documents/pmf_5.0_user_guide.pdf.

Oduber, F., Calvo, A.I., Castro, A., Blanco-Alegre, C., Alves, C., Calzolai, G., Nava, S., Lucarelli, F., Nunes, T., Barata, J., Fraile, R., 2021. Characterization of aerosol sources in León (Spain) using Positive Matrix Factorization and weather types. Sci. Total Environ. 754, 142045 https://doi.org/10.1016/J.SCITOTENV.2020.142045.

Paatero, P., Tapper, U., 1994. Positive matrix factorisation: a non-negative factor model with optimal utilization of error estimates of data values. Environmetrics 5, 111–126. https://doi.org/10.1002/ENV.3170050203.

Paglione, M., Gilardoni, S., Rinaldi, M., Decesari, S., Zanca, N., Sandrini, S., Giulianelli, L., Bacco, D., Ferrari, S., Poluzzi, V., Scotto, F., Trentini, A., Poulain, L., Herrmann, H., Wiedensohler, A., Canonaco, F., Prévôt, A.S.H., Massoli, P., Carbone, C., Facchini, M.C., Fuzzi, S., 2020. The impact of biomass burning and aqueous-phase processing on air quality: a multi-year source apportionment study in the Po Valley, Italy. Atmos. Chem. Phys. 20, 1233–1254. https://doi.org/10.5194/ACP-20-1233-2020.

Panko, J., Kreider, M., Unice, K., 2018. Chapter 7 - review of tire wear emissions: a review of tire emission measurement studies: identification of gaps and future needs. In: Amato, F. (Ed.), Non-Exhaust Emissions. Academic Press, pp. 147–160. https://doi.org/10.1016/B978-0-12-811770-5.00007-8.

Peel, M.C., Finlayson, B.L., Mcmahon, T.A., 2007. Hydrology and earth system sciences updated world map of the köppen-geiger climate classification. Hydrol. Earth Syst. Sci. 11, 1633–1644.

Pio, C., Alves, C., Nunes, T., Cerqueira, M., Lucarelli, F., Nava, S., Calzolai, G., Gianelle, V., Colombi, C., Amato, F., Karanasiou, A., Querol, X., 2020. Source apportionment of $PM_{2.5}$ and PM_{10} by Ionic and Mass Balance (IMB) in a traffic-influenced urban atmosphere, in Portugal. Atmos. Environ. 223, 117217 https://doi.org/10.1016/J.ATMOSENV.2019.117217.

Pio, C., Cerqueira, M., Harrison, R.M., Nunes, T., Mirante, F., Alves, C., Oliveira, C., Sanchez de la Campa, A., Artíñano, B., Matos, M., 2011. OC/EC ratio observations in Europe: Re-thinking the approach for apportionment between primary and secondary organic carbon. Atmos. Environ. 45, 6121–6132. https://doi.org/10.1016/J.ATMOSENV.2011.08.045.

Pio, C., Rienda, I.C., Nunes, T., Gonçalves, C., Tchepel, O., Pina, N.K., Rodrigues, J., Lucarelli, F., Alves, C.A., 2022. Impact of biomass burning and non-exhaust vehicle emissions on PM_{10} levels in a mid-size non-industrial western Iberian city. Atmos. Environ. 289, 119293 https://doi.org/10.1016/J.ATMOSENV.2022.119293.

Polissar, A.V., Hopke, P.K., Paatero, P., Malm, W.C., Sisler, J.F., 1998. Atmospheric aerosol over Alaska: 2. Elemental composition and sources. J. Geophys. Res. Atmos. 103, 19045–19057. https://doi.org/10.1029/98JD01212.

Pordata, 2021. PORDATA - Municipalities Database. https://www.pordata.pt/Municipios. (Accessed 21 March 2022) [WWW Document]. URL.

Ram, K., Sarin, M.M., 2011. Day–night variability of EC, OC, WSOC and inorganic ions in urban environment of Indo-Gangetic Plain: implications to secondary aerosol formation. Atmos. Environ. 45, 460–468. https://doi.org/10.1016/J.ATMOSENV.2010.09.055.

Ren-Jian, Z., Kin-Fai, H., Zhen-Xing, S., 2015. The role of aerosol in climate change, the environment, and human health. Atmos.and ocean. Sci. lett. 5, 156–161. https://doi.org/10.1080/16742834.2012.11446983.

Rolph, G., Stein, A., Stunder, B., 2017. Real-time environmental applications and display sYstem: ready. Environ. Model. Software 95, 210–228. https://doi.org/10.1016/J.ENVSOFT.2017.06.025.

Romano, S., Perrone, M.R., Becagli, S., Pietrogrande, M.C., Russo, M., Caricato, R., Lionetto, M.G., 2020. Ecotoxicity, genotoxicity, and oxidative potential tests of atmospheric PM_{10} particles. Atmos. Environ. 221, 117085 https://doi.org/10.1016/J.ATMOSENV.2019.117085.

Russo, A., Sousa, P.M., Durão, R.M., Ramos, A.M., Salvador, P., Linares, C., Díaz, J., Trigo, R.M., 2020. Saharan dust intrusions in the Iberian Peninsula: predominant synoptic conditions. Sci. Total Environ. 717, 137041 https://doi.org/10.1016/J.SCITOTENV.2020.137041.

Saggu, G.S., Mittal, S.K., 2020. Source apportionment of PM_{10} by positive matrix factorisation model at a source region of biomass burning. J. Environ. Manag. 266, 110545 https://doi.org/10.1016/J.JENVMAN.2020.110545.

Sainnokhoi, T.A., Kováts, N., Gelencsér, A., Hubai, K., Teke, G., Pelden, B., Tserenchimed, T., Erdenechimeg, Z., Galsuren, J., 2022. Characteristics of particle-bound polycyclic aromatic hydrocarbons (PAHs) in indoor $PM_{2.5}$ of households in the Southwest part of Ulaanbaatar capital, Mongolia. Environ. Monit. Assess. 194, 1–21. https://doi.org/10.1007/s10661-022-10297-0.

Saraga, D., Maggos, T., Degrendele, C., Klánová, J., Horvat, M., Kocman, D., Kanduč, T., Garcia Dos Santos, S., Franco, R., Gómez, P.M., Manousakas, M., Bairachtari, K., Eleftheriadis, K., Kermenidou, M., Karakitsios, S., Gotti, A., Sarigiannis, D., 2021. Multi-city comparative $PM_{2.5}$ source apportionment for fifteen sites in Europe: the ICARUS project. Sci. Total Environ. 751, 141855 https://doi.org/10.1016/J.SCITOTENV.2020.141855.

Seinfeld, J.H., Pandis, S.N., 2006. Atmospheric Chemistry and Physics : from Air Pollution to Climate Change, second ed. John Wiley Sons, New York.

Shomar, B.H., 2006. Trace elements in major solid-pesticides used in the Gaza Strip. Chemosphere 65, 898–905. https://doi.org/10.1016/J.CHEMOSPHERE.2006.03.004.

Sicard, P., Agathokleous, E., De Marco, A., Paoletti, E., Calatayud, V., 2021. Urban population exposure to air pollution in Europe over the last decades. Environ. Sci. Eur. 33, 1–12. https://doi.org/10.1186/S12302-020-00450-2/FIGURES/3.

Srivastava, D., Favez, O., Bonnaire, N., Lucarelli, F., Haeffelin, M., Perraudin, E., Gros, V., Villenave, E., Albinet, A., 2018. Speciation of organic fractions does matter for aerosol source apportionment. Part 2: intensive short-term campaign in the Paris area (France). Sci. Total Environ. 634, 267–278. https://doi.org/10.1016/j.scitotenv.2018.03.296.

Taghvaee, S., Sowlat, M.H., Mousavi, A., Hassanvand, M.S., Yunesian, M., Naddafi, K., Sioutas, C., 2018. Source apportionment of ambient $PM_{2.5}$ in two locations in central Tehran using the Positive Matrix Factorisation (PMF) model. Sci. Total Environ. 628, 672–686. https://doi.org/10.1016/J.SCITOTENV.2018.02.096.

Thomas, V.M., Bedford, J.A., Cicerone, R.J., 1997. Bromine emissions from leaded gasoline. Geophys. Res. Lett. 24, 1371–1374. https://doi.org/10.1029/97GL01243.

Thorpe, A., Harrison, R.M., 2008. Sources and properties of non-exhaust particulate matter from road traffic: a review. Sci. Total Environ. 400, 270–282. https://doi.org/10.1016/J.SCITOTENV.2008.06.007.

Uski, O., Jalava, P.I., Happo, M.S., Torvela, T., Leskinen, J., Mäki-Paakkanen, J., Tissari, J., Sippula, O., Lamberg, H., Jokiniemi, J., Hirvonen, M.R., 2015. Effect of fuel zinc content on toxicological responses of particulate matter from pellet combustion in vitro. Sci. Total Environ. 511, 331–340. https://doi.org/10.1016/J.SCITOTENV.2014.12.061.

Vecchi, R., Marcazzan, G., Valli, G., 2007. A study on nighttime-daytime PM_{10} concentration and elemental composition in relation to atmospheric dispersion in the urban area of Milan (Italy). Atmos. Environ. 41, 2136–2144. https://doi.org/10.1016/j.atmosenv.2006.10.069.

Viana, M., Reche, C., Amato, F., Alastuey, A., Querol, X., Moreno, T., Lucarelli, F., Nava, S., Calzolai, G., Chiari, M., Rico, M., 2013. Evidence of biomass burning aerosols in the Barcelona urban environment during winter time. Atmos. Environ. 72, 81–88. https://doi.org/10.1016/J.ATMOSENV.2013.02.031.

Vicente, E.D., Alves, C.A., 2018. An overview of particulate emissions from residential biomass combustion. Atmos. Res. 199, 159–185. https://doi.org/10.1016/J.ATMOSRES.2017.08.027.

Vicente, E.D., Figueiredo, D., Gonçalves, C., Lopes, I., Oliveira, H., Kováts, N., Pinheiro, T., Alves, C.A., 2021. In vitro toxicity of indoor and outdoor PM_{10} from residential wood combustion. Sci. Total Environ. 782, 146820 https://doi.org/10.1016/J.SCITOTENV.2021.146820.

Visser, S., Slowik, J.G., Furger, M., Zotter, P., Bukowiecki, N., Canonaco, F., Flechsig, U., Appel, K., Green, D.C., Tremper, A.H., Young, D.E., Williams, P.I., Allan, J.D., Coe, H., Williams, L.R., Mohr, C., Xu, L., Ng, N.L., Nemitz, E., Barlow, J.F., Halios, C. H., Fleming, Z.L., Baltensperger, U., Prévôt, A.S.H., 2015. Advanced source apportionment of size-resolved trace elements at multiple sites in London during winter. Atmos. Chem. Phys. 15, 11291–11309. https://doi.org/10.5194/acp-15-11291-2015.

Waidyatillake, N.T., Campbell, P.T., Vicendese, D., Dharmage, S.C., Curto, A., Stevenson, M., 2021. Particulate matter and premature mortality: a bayesian meta-analysis. Int. J. Environ. Res. Publ. Health 18, 7655. https://doi.org/10.3390/ijerph18147655.

Waked, A., Favez, O., Alleman, L.Y., Piot, C., Petit, J.E., Delaunay, T., Verlinden, E., Golly, B., Besombes, J.L., Jaffrezo, J.L., Leoz-Garziandia, E., 2014. Source apportionment of PM_{10} in a north-western Europe regional urban background site (Lens, France) using positive matrix factorisation and including primary biogenic emissions. Atmos. Chem. Phys. 14, 3325–3346. https://doi.org/10.5194/ACP-14-3325-2014.

Wang, J., Li, J., Ye, J., Zhao, J., Wu, Y., Hu, J., Liu, D., Nie, D., Shen, F., Huang, X., Huang, D.D., Ji, D., Sun, X., Xu, W., Guo, J., Song, S., Qin, Y., Liu, P., Turner, J.R., Lee, H.C., Hwang, S., Liao, H., Martin, S.T., Zhang, Q., Chen, M., Sun, Y., Ge, X., Jacob, D.J., 2020. Fast sulfate formation from oxidation of SO_2 by NO_2 and HONO observed in Beijing haze. Nat. Commun. 11, 1–7. https://doi.org/10.1038/s41467-020-16683-x.

Wang, T., Liu, Y., Cheng, H., Wang, Z., Fu, H., Chen, J., Zhang, L., 2022. Significant formation of sulfate aerosols contributed by the heterogeneous drivers of dust surface. Atmos. Chem. Phys. 22, 13467–13493. https://doi.org/10.5194/acp-2022-227.

Weber, S., Salameh, D., Albinet, A., Alleman, L.Y., Waked, A., Besombes, J.-L., Jacob, V., Guillaud, G., Meshbah, B., Rocq, B., Hulin, A., Dominik-Sègue, M., Chrétien, E., Jaffrezo, J.-L., Favez, O., 2019. Comparison of PM_{10} sources profiles at 15 French sites using a harmonized constrained Positive Matrix Factorisation approach. Atmos 10, 310. https://doi.org/10.3390/atmos10060310.

Winid, B., 2015. Bromine and water quality – selected aspects and future perspectives. Appl. Geochem. 63, 413–435. https://doi.org/10.1016/J.APGEOCHEM.2015.10.004.

Yang, X., Yan, J.I., Wang, F., Xu, J., Liu, X., Ma, K.E., Hu, X., Ye, J., 2016. Comparison of organics and heavy metals acute toxicities to Vibrio fischeri. J. Serb. Chem. Soc. 81, 697–705. https://doi.org/10.2298/JSC151124011Y.

Yu, K.N., Cheung, Y.P., Cheung, T., Henry, R.C., 2004. Identifying the impact of large urban airports on local air quality by nonparametric regression. Atmos. Environ. 38, 4501–4507. https://doi.org/10.1016/J.ATMOSENV.2004.05.034.

Zong, Z., Wang, X., Tian, C., Chen, Y., Fu, S., Qu, L., Ji, L., Li, J., Zhang, G., 2018. PMF and PSCF based source apportionment of PM2.5 at a regional background site in North China. Atmos. Res. 203, 207–215. https://doi.org/10.1016/J.ATMOSRES.2017.12.013.